FINAL REPORT
U.S. Department of Energy

Molecular-Level Processes Governing the Interaction of Contaminants with Iron and Manganese Oxides

Principle Investigators:

S.A. Chambers, Environmental Molecular Sciences Laboratory, Pacific Northwest National Laboratory (PNNL), PO Box 999, MS K8-93, Richland, WA 99352.
(509) 376-1766, sa.chambers@pnl.gov

G.E. Brown, Jr., Stanford University, Department of Geological and Environmental Sciences, and Stanford Synchrotron Radiation Laboratory (SSRL), Stanford, CA 94305-2115.
(650) 723-9168, gordon@pangea.stanford.edu

Contributors:

J.E. Amonette (PPNL), *N.S. Foster-Mills* (PPNL), *S.A. Joyce* (PPNL), *T.J. Kendelewicz* (SSRL), *J.R. Rustad* (PNNL), *S. Thevuthasan* (PNNL)

Project Number: 54635

Grant Number: DE-AC06-76RLO-1839 (PNNL)
FG07-98ER14842 (Stanford)

Grant Project Officers: Dr. Roland Hirsch

Project Duration: October 1, 1996 – October 1, 1999

Table of Contents

I. Executive Summary……. 3

II. Research Objective……. 4

III. Methods, Results, Impact and Relevance…… 4-27

A. Introduction…… 4-5
B. Epitaxial growth and characterization of model iron oxide surfaces By oxygen-plasma-assisted molecular beam epitaxy…… 6-7
C. Interaction of water vapor and bulk water with iron oxide surfaces……. 7-10
D. Molecular simulations of iron oxide surfaces before and after Interaction with water……. 10-15
E. Chromium sorption products on reduced hematite and magnetite surfaces…… 15-19
F. The nature of the reacted layer and kinetics of $Cr(VI)_{aq}$ reduction Reaction of magnetite surfaces……. 19-23
G. $Cr(VI)_{aq}$ sorption on hematite surfaces in the presence of phosphate And sulfate……. 23-27

IV. Conclusions……. 27-28

V. Appendices…… 29-38

A. References (including all papers published under the auspices of this program…… 29-31
B. Project Productivity……. 32
C. Personnel Supported…… 32
D. Interactions…….. 32-37
E. Future Work……. 37-38

I. Executive Summary

We have studied the interaction of aqueous chromate with well-defined iron oxides solid surfaces in order to determine the extent to which such minerals bind and immobilize chromate. Chromate is a highly carcinogenic and bioavailable contaminant found in soil and groundwater at many DOE sites. Naturally occurring iron oxide mineral surfaces may have the potential of bonding to aqueous chromate and chemically modifying it to a form that is less toxic, mobile, and bioavailable. Testing this hypothesis, and gaining a molecular-level understanding of the process (if it occurs), were two of our primary goals of this project. Our research shows that iron-bearing minerals containing iron in the +2 oxidation state do indeed bind and chemically reduce chromium in chromate from the +6 to the +3 oxidation state. The resulting species, chromium in the +3 oxidation state surrounded by water molecules on all sides, except the side facing the mineral surface, is less toxic and more strongly bound to the mineral surface than chromate. However, the phenomenon is strictly a surface effect, in that once a particular surface binds and converts an ~1.5 nanometer thick layer of chromate, the reaction stops and no more chemical transformation of chromate to the less harmful form can occur. Our results are directly applicable to the so-called "zero-valent iron" remediation technology, in that the surface of iron shavings consists a thin skin of iron oxide containing iron in the +2 oxidation state. Therefore, with respect to chromate immobilization and reduction, zero-valent iron is expected to be useful, but only in a high-surface-area form. Finally, we have developed a versatile instrument, called a laser photoacoustic spectrometer, to study competitive uptake of ions from solution by mineral surfaces in real time. In the context of the present project, this instrument was used to investigate competitive uptake of chromate and nontoxic phosphate and sulfate by iron oxide mineral powder. However, the instrument is broadly applicable to the study of a wide range of ion/mineral-surface interactions.

II. Research Objective

The central tenet of this program is that *a fundamental understanding of specific mineral surface-site reactivities will substantially improve reactive transport models of contaminants in geologic systems, and will allow more effective remediation schemes to be devised.* To this end, we carried out a program of research that focuses on the fundamental mechanisms of redox chemistry of contaminants on mineral surfaces. As much of this chemistry in sediments involves the Fe(III)/Fe(II) couples, we focussed on mineral phases containing these species. Our approach was to conduct carefully controlled experiments on model, single-crystal Fe oxide mineral surfaces grown by molecular beam epitaxy, natural Fe oxide single crystals, and synthetic mineral powders. We used the results from the model surfaces, which were very well defined in terms of surface composition, structure, and defect densities, to understand the results obtained on more complex mineral specimens. We used a variety of experimental probes, along with molecular modeling theory, to determine clean mineral surface structure, details of the chemisorption and decomposition of water, and the interface structure and redox chemistry of important contaminants such as CrO_4^{-2} on these surfaces. Our approach has been highly novel and innovative in that our is the only such effort to utilize state-of-the-art thin film growth techniques to prepare model surfaces of iron and manganese containing minerals.

III. Methods and Results

A. Introduction

Redox-sensitive inorganic and organic contaminants present in sediments at DOE sites can be altered or destroyed by electron transfer reactions occurring abiotically on mineral surfaces. One such contaminant is chromium, which can exist in 6+, 3+, 2+, and 0 oxidation states (*1*), depending upon conditions. Over the pH range of most natural groundwaters, Cr(III) is thermodynamically more stable as a sorbed surface complex or a solid (oxy)hydroxide precipitate than as an aqueous complex (*2*). Therefore, the small environmental hazard posed by Cr(III) tends to be localized to the region where it has sorbed or precipitated. In contrast, $Cr(VI)_{aq}$ is thermodynamically stable as anionic solution species, in the absence of a reductant such as Fe(II), over the same pH range where Cr(III) species tend to precipitate. These differences make $Cr(VI)_{aq}$ the more mobile and, potentially, the more bioavailable of the two most common oxidation states of chromium. $Cr(VI)_{aq}$, is also the more toxic form of Cr (*3*).

A fundamental understanding of abiotic surface redox processes provided by molecular-level studies on structurally and compositionally well-defined mineral surfaces is needed to improve predictive models of the fate and transport of chromium in geochemical systems and to optimize manipulation of these processes for remediation purposes. Toward this end, we have undertaken a program of research designed to answer the following questions:

1. What are the structures of clean iron oxide surfaces that might react with $Cr(VI)_{aq}$?
2. How does water interact with these surfaces?

3. What are the reaction products when $Cr(VI)_{aq}$ interacts with reduced hematite and magnetite surfaces, and what effect do they have on the Cr(VI) to Cr(III) reduction process?
4. What are the kinetics of this reduction reaction and how are they affected by solution pH and the build-up of reaction products on the surface?
5. Do other common aqueous oxoanions such as HPO_4^{2-} and SO_4^{2-} interfere with $Cr(VI)_{aq}$ sorption on iron oxides?

We have utilized both synthetic and natural hematites and magnetites in this work and have characterized their surfaces using x-ray photoemission spectroscopy (XPS), low-energy electron diffraction (LEED), reflection high-energy electron diffraction (RHEED), x-ray photoelectron diffraction (XPD), and vacuum scanning tunneling microscopy (STM). The clean model surfaces were reacted with water vapor under ultrahigh vacuum (UHV) conditions and the reaction products were characterized by O 1s photoemission. Molecular simulations were used to predict the structures of hematite and magnetite surfaces before and after interaction with water. Reaction products resulting from the interaction of $Cr(VI)_{aq}$ with iron oxide surfaces were studied under ambient conditions using grazing-incidence Cr K-edge x-ray absorption fine structure (XAFS) spectroscopy and under UHV conditions using Cr and Fe L-edge and O K-edge x-ray absorption and O 1s, Cr 2p, and Fe 2p photoemission. Reaction kinetics were also studied by monitoring changes in the Cr 2p, Fe 2p, and O 1s photoemission spectra. Finally, the competitive effects of aqueous HPO_4^{2-} and SO_4^{2-} on CrO_4^{2-} sorption on powdered hematite were studied by laser photoacoustic spectroscopy and batch uptake experiments.

B. Epitaxial Growth and Characterization of Model Iron Oxide Surfaces by Oxygen-Plasma-Assisted Molecular Beam Epitaxy

In order to produce the full range of iron oxide phases and crystal surface orientations required for studies of $Cr(VI)_{aq}$ reduction reactions, we used oxygen-plasma-assisted molecular beam epitaxy (OPA-MBE) to prepare well-defined epitaxial films (≈ 300-500 Å thick) on two kinds of oxide substrates – α-Al_2O_3 for α-Fe_2O_3 (*4-10*) and MgO for Fe_3O_4, α-Fe_2O_3 and $Fe_{1-x}O$ (*4,7,8,10-13*). The lattice mismatches for α-Fe_2O_3 on α-Al_2O_3, Fe_3O_4 on MgO, α-Fe_2O_3 on MgO and $Fe_{1-x}O$ on MgO are +5.8%, –0.38%, –0.89%, and +2.30%, respectively, after taking into account the factor-of-two difference in lattice parameter between Fe_3O_4/α-Fe_2O_3 and MgO. Fe_3O_4 can be used as an interlayer between $Fe_{1-x}O$ and MgO to distribute the strain (*12*). Fe_3O_4(111) has been grown on α-Al_2O_3(0001), although the sizeable lattice mismatch (+8.1%) results in the nucleation of rotational domains with equal populations (*4*). It is, in principle, possible to grow Fe_3O_4, α-Fe_2O_3 and $Fe_{1-x}O$ on MgO(110), although facetting on this surface results in poor film quality and rough surfaces. The Fe_3O_4/MgO and α-Fe_2O_3/MgO interfaces are thermodynamically unstable, leading to cation interdiffusion. The full range of iron oxide stoichiometries can be reached in OPA-MBE by adjusting the relative Fe and activated oxygen fluxes at the substrate. Figure 1 shows an empirically derived phase diagram that illustrates these values (*12*). Points on the border between Fe_2O_3 and Fe_3O_4 represent growths that resulted in a mixed phase in the film.

The relatively large compressive lattice mismatch for α-Fe_2O_3 on α-Al_2O_3 leads to the formation of a heavily strained wetting layer of fully stoichiometric α-Fe_2O_3 that is

buckled along the [1-102] direction, provided the first several tens of Å are grown at an exceedingly slow rate (~1 Å/min) at a substrate temperature of 450°C (*9*). This strained layer then transforms to 3-D nanocrystals above a coverage of a few ML. A higher initial growth rate (such as 6 Å/min) kinetically impedes the critically important transition from strained layer-by-layer to relaxed 3-D island formation that leads to the nucleation of well-ordered epitaxial α-Fe_2O_3(0001). Instead, a γ-Fe_2O_3–like epilayer is nucleated and exhibits domains with 180° rotational twinning and surface orientations that deviate substantially from (111) (*14*). The formation of single-phase α-Fe_2O_3 does not occur once this γ-Fe_2O_3–like layer has nucleated. These 3-D islands, or nanocrystals, gradually coalesce with film thickness into what looks by all probes except high-resolution x-ray diffraction to be a single crystal with a reasonably flat surface. STM images of a partially conductive α-Fe_2O_3(0001) film that was doped with Fe(II) (not shown) reveal typical terrace widths of a few tens of Å's, and terraces that are separated by ≈ 2 Å high steps. This step height is the difference between structurally equivalent planes in the α-Fe_2O_3(0001) structure. Thus, the surface consists of a single termination.

Figure 1. Phase diagram for the growth of iron oxides by OPA-MBE. Taken from 12.

XPD results established that the terminating plane is that of a single 1/3 ML of Fe, which is the only autocompensated and, therefore, stable termination of α-Fe_2O_3(0001)

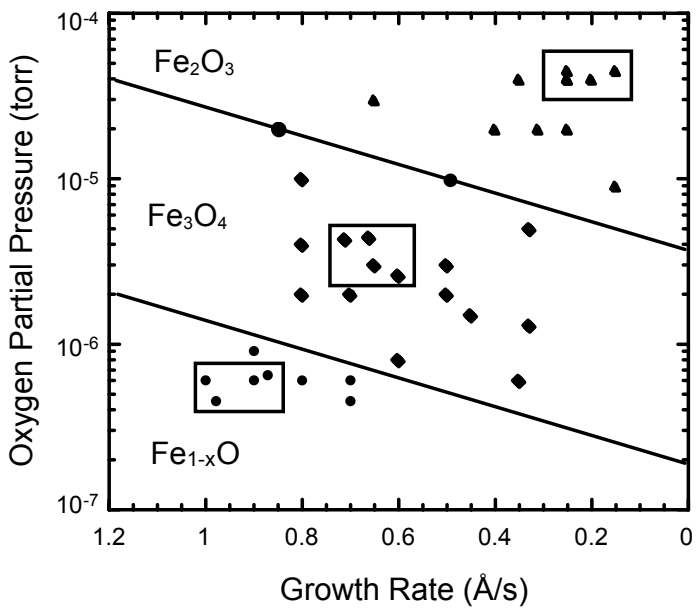

(*15*). This result is at odds with that of Wang et al., whose spin-DFT calculations and STM images suggest that both the 1/3 ML Fe and O terminations can be stabilized on this surface (*16,17*). MBE growth of Fe_3O_4(100) on MgO(100) has produced surfaces that are readily imaged by STM with atomic resolution due to the high electrical conductivity of Fe_3O_4 at room temperature (*18-24*). However, there has been some controversy and ambiguity concerning the interpretation of these images. For instance, Gaines et al. observed elongated images at the corners of a primitive square that these authors interpreted as being due to tetrahedral Fe(III) dimers in the terminal layer (*21*). Similar

elongated images were seen earlier on the surface of natural $Fe_3O_4(100)$ crystal by Terrach et al. (*25*). However, this surface structure requires a full ML of tetrahedral Fe(III). Such a surface is not autocompensated and, therefore, has a non-zero surface dipole and the associated instability. In contrast, we did not see evidence for elongation in the Fe atom images and thus interpreted them as being due to single tetrahedral Fe(III) cations in the top layer (*23*). This interpretation requires that the top layer be composed of 1/2 ML of tetrahedral Fe(III) in which every other Fe is missing. This surface structure constitutes a $(\sqrt{2}x\sqrt{2})R45°$ surface net, which matches both RHEED and LEED patterns. Such a surface is autocompensated and has no dipole moment. These results suggest that the most stable surface is that terminated with tetrahedral Fe(III). However, Voogt first suggested that the octahedral Fe/tetrahedral O terminal layer would also be autocompensated and, therefore, stable if there were a modification in the distribution of Fe oxidation states in the octahedral plane, and an ordered array of O vacancies (*26*). Subsequently, Stanka et al. observed that such a surface can be routinely stabilized with MBE-grown $Fe_3O_4(100)$ specimens that are transferred through air and cleaned under somewhat oxidizing conditions (*24*). Figure 2 shows STM images of $Fe_3O_4(100)$ illustrating the two terminations – (a) tetrahedral Fe, representative of the as-grown surface (*23*) and, (b) octahedral Fe/tetrahedral O termination on specimens transferred under vacuum from the MBE chamber to an STM chamber at Tulane University in the laboratory of Professor Ulrike Diebold (*24*). It is currently not understood why the different terminations seem to arise rather exclusively under different preparation conditions. What can be said at this point is that both terminations are autocompensated and, therefore, expected to be stable in vacuum.

C. Interaction of Water Vapor and Bulk Water with Iron Oxide Surfaces

Prior to exposure of the hematite and magnetite surfaces to $Cr(VI)_{aq}$, we undertook a study of the interaction of deionized water vapor with the clean surfaces of hematite (0001) and magnetite (100) and (111) using O 1s photoemission on wiggler beam line 10-1 at the Stanford Synchrotron Radiation Laboratory (SSRL). The purpose of these experiments was to gain insights about the electronic structure and nature of the water-exposed vs. clean magnetite and hematite surfaces without the complication of $Cr(VI)_{aq}$ ions. The hematite samples were (0001) surfaces of thin-film α-Fe_2O_3 ($\approx$ 300 Å thick) grown on an α-Al_2O_3 (0001) substrate by the MBE methods described earlier, whereas the magnetite (100) samples were cut and polished (using 300 μm grit α-alumina) from natural single crystal magnetites. The magnetite (100) surfaces were cleaned using several cycles of Ar^+ sputtering and annealing in vacuum at 700°C for 1 to 10 hours. These surfaces showed normal LEED patterns following cleaning and no XPS evidence of adventitious carbon. The hematite (0001) surfaces were cleaned by several cycles of annealing in 10^{-5} torr oxygen at 500-800°C for 30 min., without Ar^+ sputtering, and showed good 1 x 1 LEED patterns following cleaning and no XPS evidence of adventitious carbon. The water dosing experiments were conducted by exposing each surface to sequential doses of water vapor at pressures, $p(H_2O)$, ranging from 10^{-9} torr to 10 torr, at a constant reaction time (3 min.) and, in separate experiments, at

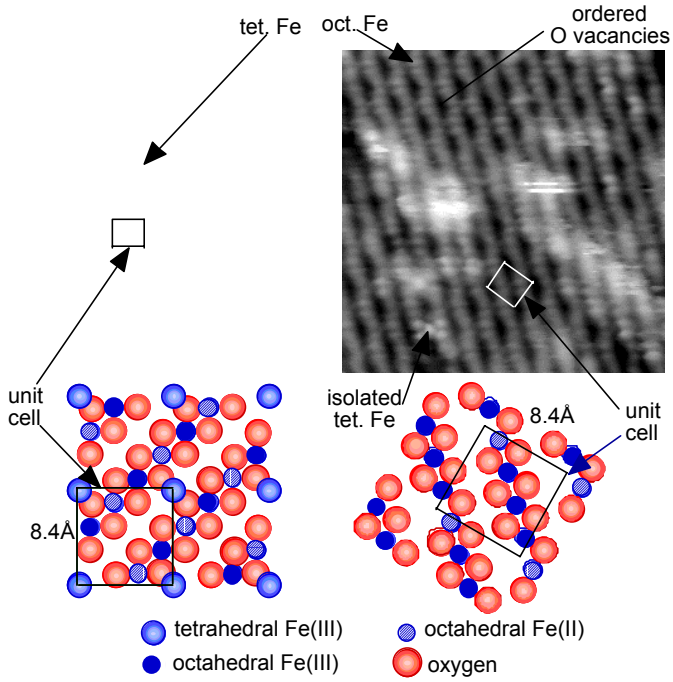

Figure 2. STM images of (√2x√2)R45° Fe_3O_4/MgO(100) grown by OPA-MBE showing: (a) the tetrahedral Fe termination, and (b) the octahedral Fe/tetrahedral O termination, with an ordered array of oxygen vacancies. Taken from 23 (a) and 24 (b).

longer reaction times (≤ 30 min., with total exposures ranging from 1.8 Langmuir (1L = 10^{-6} torr sec) to 1.8 x 10^{10} L) at constant p(H_2O). The doubly deionized water used in these experiments was degassed by several freeze-pump-thaw cycles and was introduced into the UHV chamber using a precision leak valve. These water-dosing experiments were conducted in a preparation chamber attached to our main UHV analysis chamber, which operated at a base pressure of 1 x 10^{-10} torr. The O 1s photoemission spectra were obtained using a 1000 line/mm grating, entrance and exit slits of 50 µm, and incident photon energies of 630 or 650 eV, which are near the minimum of the universal curve, thus very surface sensitive. Additional details about these experiments can be found in (*27*) for the magnetite surfaces and in (*28*) for the hematite surfaces.

Changes in the electronic structure of magnetite (100) and (111) surfaces were examined after reaction with water vapor at p(H_2O) ranging from 10^{-9} to 9 torr and with liquid water at 298 K using chemical shifts in the O 1s core-level photoelectron spectra measured on BL 10-1 at SSRL. Oxygen 1s photoemission data are shown for the magnetite (100) surface in Figure 3 and consist of a lattice oxygen feature at higher kinetic energy and a second feature shifted by 1.2 to 2.5 eV to lower kinetic energy. Similar results were obtained for the magnetite (111) surface. We attribute this lower kinetic energy feature to OH groups resulting from dissociative chemisorption of water on the magnetite surface. The range of chemical shifts observed is attributed to a range of surface hydroxyl sites with different binding energies (*27*). We found that the p(H_2O) at which water first reacts with magnetite is similar for the two surfaces (≤ 10^{-5} torr for 3

min. exposures, corresponding to doses of $\leq 1.8 \times 10^3$ L) and is consistent with a small sticking coefficient and hydroxylation of defect sites. The $p(H_2O)$ for the onset of an extensive hydroxylation reaction is $\approx 10^{-3}$ Torr (3 min. dose or $\approx 1.8 \times 10^5$ L). Magnetite (100) and (111) surfaces exposed to higher $p(H_2O)$ react more extensively, with hydroxylation extending several layers (≈ 8 Å) deep into the bulk. Comparison of O KVV Auger K-edge absorption spectra of water vapor-exposed magnetite (100) and (111) surfaces with the corresponding total yield spectra of goethite (α-FeOOH), limonite ($FeOOH \bullet nH_2O$), and hematite (α-Fe_2O_3) (not shown) shows that the reaction product on the magnetite surfaces is not goethite, limonite, or hematite (*27*). In addition, similarity of the Fe $L_3M_{23}M_{23}$ Auger yield L-edge absorption spectra before and after exposure of the magnetite (111) surface to liquid water (not shown) indicates that the oxidation state of iron is unchanged (*27*). We also measured O 1s chemical shifts on magnetite (111) surfaces that had been immersed in liquid water. These spectra also showed evidence for extensive surface hydroxylation.

Annealing experiments to temperatures of 700°C did not cause significant loss in intensity of the OH photoemission feature from the water-dosed magnetite surfaces. These results indicate that the hydroxyls are strongly bound to the surface. We also observed a shift in the centroid of the OH component to higher kinetic energies with annealing, and interpret this result as indicating a loss of the most weakly bound surface hydroxyls (*27*).

Our O 1s photoemission results for hematite(0001) are similar to those for the two magnetite surfaces. A two-stage reaction was observed for the hematite (0001) surface, with dissociative chemisorption of water occurring mainly at defect sites below a threshold pressure of $\approx 10^{-4}$. The percentage of defects on this surface estimated from the low water dosage experiments is 5 - 10%. Extensive hydroxylation of this surface was found to occur above the threshold pressure. Longer water vapor exposures below the threshold pressure did not result in significant increases in hydroxylation; however, longer exposures above the threshold pressure resulted in increased hydroxylation. The measured threshold pressure for hematite is more than five orders of magnitude lower than the threshold pressure for the conversion of hematite to α-FeOOH or $Fe(OH)_3$ predicted from equilibrium thermodynamics (*28*). This difference between observation and prediction for hematite (0001) is not completely understood, but may be due to the presence of a passivating layer of Fe-(oxy)hydroxide that reduces the surface energy of the hydroxylated hematite (0001) surface (*28*).

These results, coupled with those from our studies of the interaction of water with MgO(100) (*29,30*), and α-Al_2O_3(0001) (*28*) and with molecular mechanics studies of the interaction of water molecules with MgO (*31*) and α-Al_2O_3 (*32*), lead to the suggestion that extensive dissociative chemisorption of water on terrace sites on these surfaces is, in part, a function of the water coverage. The "threshold" $p(H_2O)$ values observed for these metal oxide surfaces (10^{-4} to 10^{-3} torr) correspond to coverages of about 0.5-0.6 monolayers, which is about the same coverage found in the theoretical studies that resulted in significant interaction between adjacent water molecules. Such intermolecular interactions appear to be necessary for the dissociation of water on these surfaces.

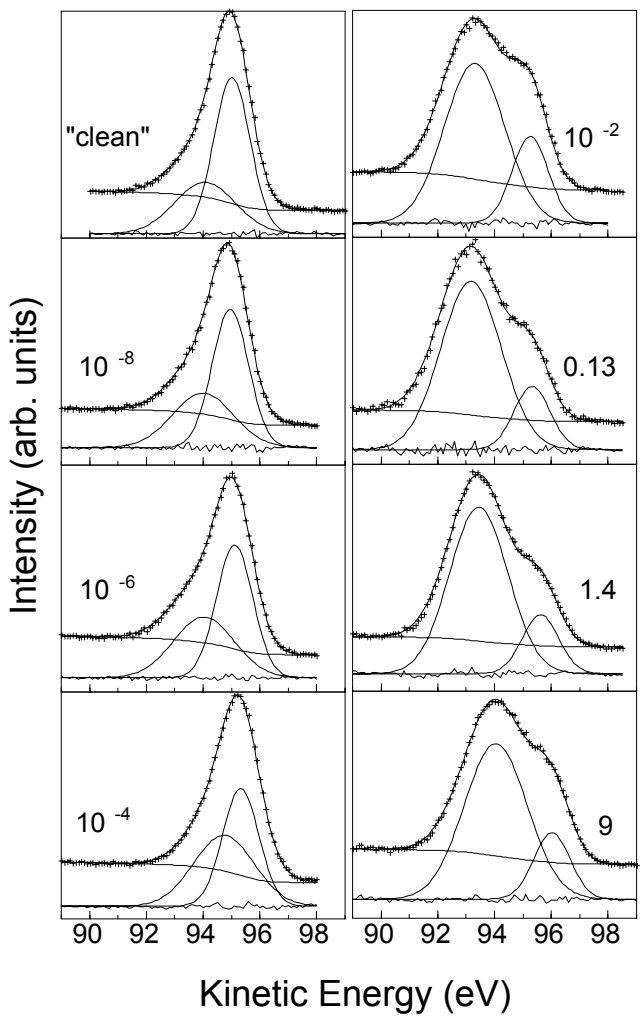

Figure 3. Oxygen 1s photoemission spectra of the (100) magnetite surface, using 630 eV incident photons, before and after sequential doses of water vapor, at the doses indicated in torr (3 min. exposures at each dose). From (27).

D. Molecular Simulations of Iron Oxide Surfaces Before and After Interaction with Water

In an effort to simulate the surface structures of clean and hydroxylated magnetite and hematite, molecular modeling calculations were carried out, and the results are compared with those from our photoemission and x-ray photoelectron diffraction studies discussed in previous sections.

1. Potential Model

The model for pair potentials employed in our molecular simulations is an ionic one that was originally designed to calculate structures and energies for hydroxylated/hydrated ferric oxide surfaces. The O-H potential functions were taken from the polarizable, dissociating water model of Halley and co-workers (*33*), which is a

variant of the Stillinger-David model (*34*). The Fe-O parameters, including a short-range repulsion and charge-dipole cutoff functions, were fit to the Fe^{3+}-H_2O potential surface of Curtiss and co-workers (*35*). This model has been used in a variety of applications including simulations of ion hydrolysis in solution (*36*), ferric oxide and (oxy)hydroxide crystal structures (*37*), the vacuum termination of hematite (0001) (*38*), monolayers of water on hematite (1-102) (*39,40*), and the surface charging behavior of goethite (α-FeOOH) and hematite (*41,42*).

2. Simulation of the Hydroxylation of the Hematite Surfaces

In our simulation of the hematite (0001) surface (*42*), excellent predictions were obtained for surface relaxation in good agreement with experiment (*6*) and later high level LAPW *ab initio* calculations (*43*). The surface energy from our simulations also compared favorably with the LAPW *ab initio* calculations. The extent of hydroxylation of the hematite (1-102) surface was also in good agreement with experimental studies. The adsorption energy for water as a function of extent of hydroxylation, taken from a search of over 1200 configurations is shown in Figure 4.

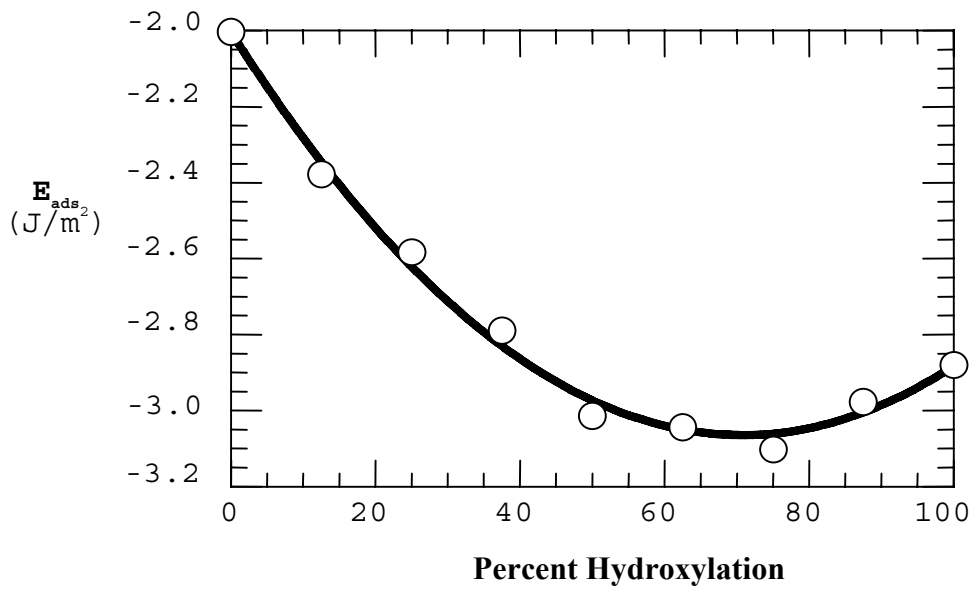

Figure 4. Calculated adsorption energy of water molecules at 100 percent coverage on the (1-102) surface of hematite as a function of the amount of hydroxylation. From ***(40)****.*

3. Simulation of Magnetite Surfaces

More recently, the same potentials were applied to magnetite (*44*). In this work, it was shown that a reasonable structural model for magnetite and wustite could be obtained simply by changing the Fe charge to 2.5+ or 2+, keeping the same short-range repulsive and charge-dipole cutoff function parameters. As is the case for the ferric oxide structures, the Fe-O bond was found to be approximately 5 percent too long. For

example, the Fe^{2+}-O distance in $Fe(H_2O)_6^{2+}$ was predicted to be 2.21 Å, as opposed to the experimental value of 2.15 Å. High-level quantum mechanical calculations give 2.19 Å (*45*). It appears that going beyond our rather crude description of the Fe-O bond may be difficult for *ab initio* methods. Given our good agreement with experiment as outlined above, and in view of the electronic structural complexity of magnetite (resulting in formidable challenges in applying *ab initio* methods), it is justifiable to continue to explore the predictions of this simple model.

a. Simulations on the "A" Termination of Magnetite (100)

The relaxed structure for the "A" termination of magnetite (100) was calculated in (*44*). The surface is predicted to undergo significant surface relaxation involving the rotation of the two-fold coordinated irons into the adjacent octahedral vacancies exposed at the surface. At the same time the bulk tetrahedral ferric ions, which share a face of their coordination polyhedron with the surface half-octahedron newly occupied by the relaxing surface ferric irons, are themselves pushed to the surface, yielding a sequence of ferric "dimers" as shown in Figure 5. The driving force for the relaxation is the reestablishment a Pauling bond order of 2.0 v.u. for the surface oxygens, some of which have become significantly over and undercoordinated at the unrelaxed surface. This is essentially the same reasoning as that discussed earlier involving the autocompensation concept. The relaxation energy associated with the reconstruction is approximately 0.72 J/m^2, which is quite significant given that the unrelaxed surface energy is about 2.3 J/m^2. The dimers formed on the surface provide a compelling interpretation of STM images showing "dimeric" structures.

b. Simulations on the "B" Termination of Magnetite (100*)*

The "B" or octahedral termination of magnetite (100) has been discussed in (*26*), and predictions of its structure stability were made in (*46*). The simplest way to envision this termination is (within each unit cell):

1) remove 1/2 e^- from two of the $Fe^{2.5+}$ in the octahedral sites to give Fe^{3+} sites.
2) place the electron on the tetrahedral Fe^{3+} site to make an Fe^{2+} site.
3) remove FeO from the system by taking the tetrahedral Fe^{2+} site and creating an oxygen vacancy.

The surface is neutral; stoichiometric FeO was removed. The "B" termination is therefore oxidized relative to Fe_3O_4 and the relative stabilities of the "A" and "B" terminations will depend on the oxygen fugacity in the system. Note that both surfaces maintain the $(\sqrt{2}\times\sqrt{2})R45°$ unit cell characteristic of the neutral stacking units. This cell is in fact observed in LEED patterns of magnetite (100) for both "A" and "B" terminations (*11,47*).

If the "B" surface is generated from the "A" surface using the three-step recipe listed above, the octahedral sites are treated as a mixture of equal numbers of $Fe^{2.5+}$ and Fe^{3+} sites, as shown in Figure 5. Maintaining the policy, for the present, of keeping the electrons delocalized, this mixture of $Fe^{2.5+}$ and Fe^{3+} sites is treated as if all surface irons have a charge of +2.75. Each of the three different possibilities for creation of the oxygen vacancy was tested. In the lowest energy structure, the O atom adjacent to the

vacancy moves into a bridgeposition with respect to the two Fe^{3+} irons at the surface. This small relaxation contributes less than 0.1 J/m^2 to the slab energy. The $(\sqrt{2}\times\sqrt{2})R45°$ symmetry is maintained during the surface relaxation.

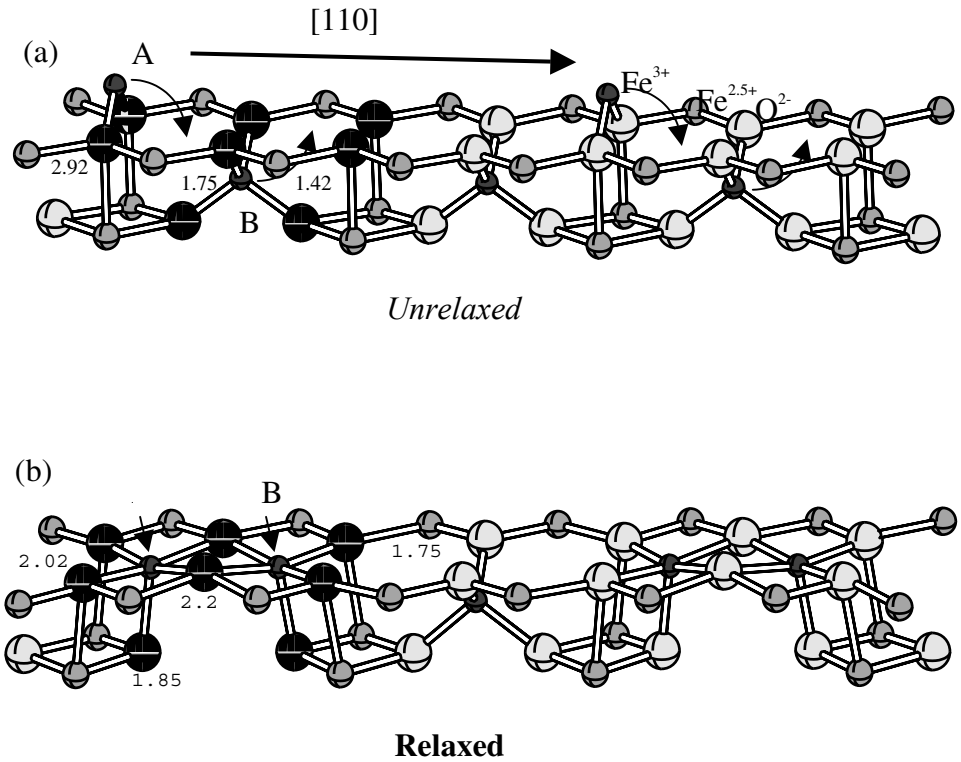

Figure 5. Atomic rearrangements during relaxation of the vacuum-terminated magnetite (100) surface. Pauling bond strengths in valence units (v.u.) are given on the figure for the "active" oxygen atoms. In the bulk, the net contribution to each oxygen atom is 2 v.u. From (44).

4. Relative Energetics of the "A" and "B" Terminations of Magnetite (100)

a. Vacuum Terminated Surfaces

In (*46*) the relative stabilities of the "A" and "B" terminations of magnetite (100) were assessed. It was necessary to model the surface with a charge-ordered slab, rather than using a non-integral charge on the octahedral sites, to maintain consistency with energy calculations on Fe^{3+} and Fe^{2+} solids. For example, the energy of charge-ordered magnetite (with Fe^{3+} and Fe^{2+} B sites) will always be lower than the energy of charge-disordered magnetite (with $Fe^{2.5+}$ B sites). This arises from the lack of quantum mechanical effects favoring charge delocalization (such as electron kinetic energy). The model system described here therefore differs from that described in (*44*) in that the system is charge-ordered. Because no attempt was made to self-consistently calculate the charge distribution, the simple charge-ordering scheme in Hamilton (*48*) was used, with Fe^{3+} and Fe^{2+} alternating in layers perpendicular to [100]. In either the "A" or "B"

terminations, the terminating surface could consist of either Fe^{2+} or Fe^{3+} ions. Because, within the context of our model, the Fe^{2+} ions prefer to be at the surface, we choose the former arrangement. For this arrangement, the relaxation of the surface tetrahedral iron atoms is the same as in the charge-delocalized arrangement as described in (*44*). The structure of the "B" termination is also essentially unchanged from the charge-disordered case. We note that if the higher energy Fe^{3+} termination is used to model the surface, the relaxation mechanism identified in (*44*) does not occur due to crowding of ferric iron in the first layer.

For non-stoichiometric systems, calculation of the surface energies cannot be carried out in the standard way, according to the formula $\gamma = 1/2A(E_{slab}-E_{bulk})$, where A is the area of the slab, E_{slab} is the energy of the slab and E_{bulk} is the bulk energy of an equivalent number of formula units in the bulk. The issue, of course, is that for the nonstoichiometric "B" surface, there is no "bulk" value against which to reference the slab energy. A similar problem was addressed by Wang and coworkers (*43*) in their study of nonstoichiometric terminations of hematite (001). In (*46*) a similar approach was taken, but was modified to overcome the constraints of using the ionic model. Energies for O_2 or metallic iron cannot be calculated with an ionic model, and the oxygen fugacity was fixed through calculation of the energies of hematite and wustite and knowledge of the experimental oxygen fugacities at the hematite-magnetite, and metastable magnetite-wustite, and hematite-wustite buffers. This allows calculation of the surface energy of the model slab as a function of oxygen pressure (*44*) and, hence, of the relative energies of the "A" and "B" terminated slabs over the entire range of accessible conditions. As shown in Figure 6, the "A" termination is stable relative to the "B" termination over the entire range of P_{O2} examined. As a caveat, we remark that this calculation will depend to some extent on the possibility of rearranging charge in going from the "A" to the "B" termination. We have ignored this possibility.

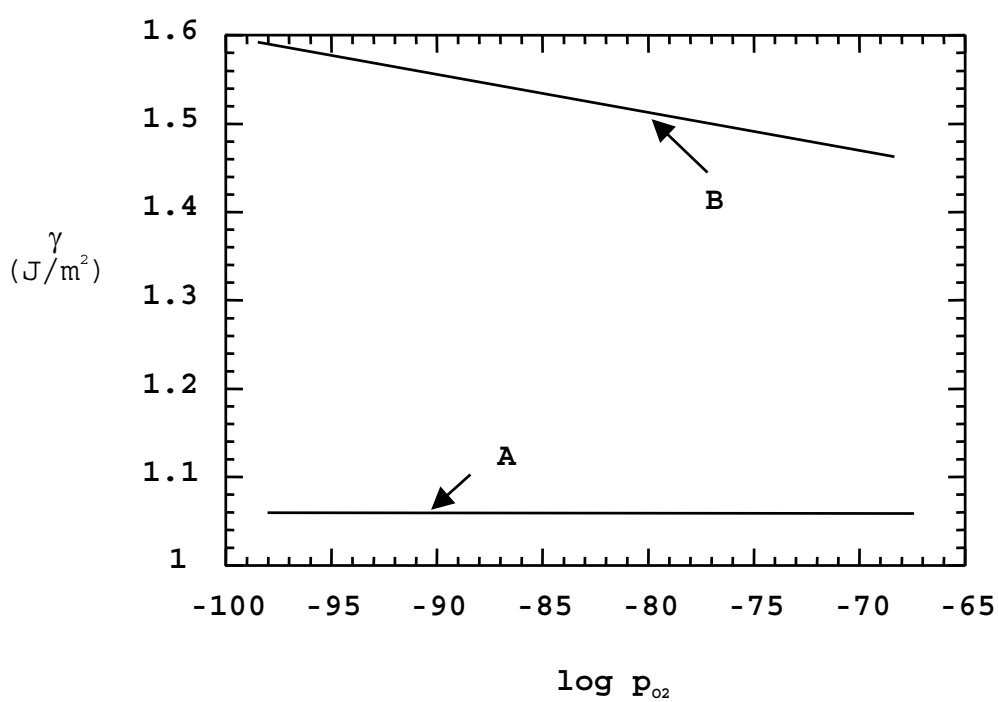

Figure 6. Relative energies of the "A" and "B" terminated magnetite (100) surfaces using the charge ordering scheme from (48) with Fe^{2+} ions in the surface layer. From (46).

b. Hydroxylated Surfaces of Magnetite (100)

In (*46*) calculations were carried out on three sets of hydroxylated slabs, including both the relaxed and unrelaxed "A" terminations, and the "B" termination. For the "A" termination, four waters were added per unit cell to the octahedral sites and two waters per unit cell were added to the tetrahedral sites. An exhaustive search through the possible surface tautomers yielded the structure shown in Figure 7a. An analogous investigation for the "B" terminated surface yielded the structure shown in Figure 7b. Total water binding energies for both surfaces are about 2.32 J/m^2, indicating that the water will have little effect, at least in a thermodynamic sense, on which surface is observed. It was also shown in (*46*) that hydroxylation stabilizes the unrelaxed magnetite (100) structure as opposed to the relaxed structure as identified in (*44*).

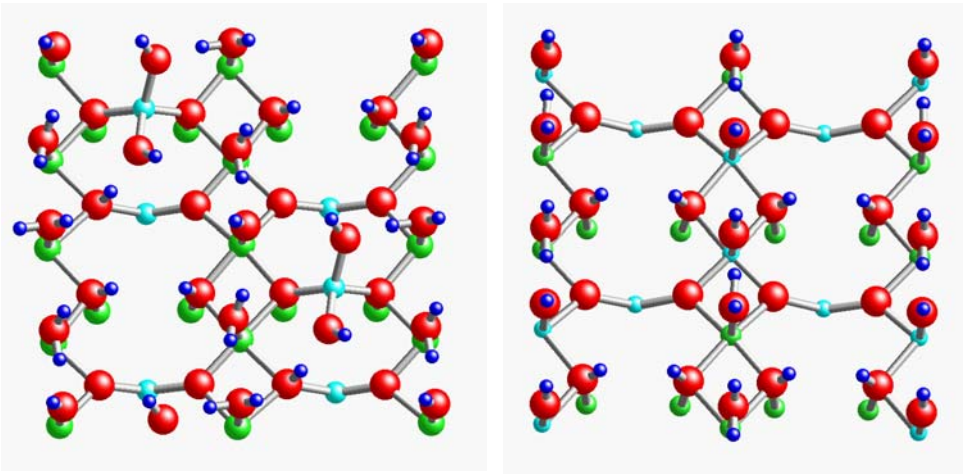

(a) (b)

Figure 7. Minimum energy tautomeric forms for the hydroxylated "A" (a) and "B" (b) terminations of the magnetite (100) suface. Note that in the minimum energy structure for "A", tetrahedral sites revert back to the unrelaxed configuration (see Fig. 5). From (46).

E. Chromium Sorption Products on Reduced Hematite and Magnetite Surfaces

One of the main objectives of our DOE-EMSP-funded research was to gain an improved molecular-level understanding of the reduction of $Cr(VI)_{aq}$ on the surfaces of Fe(II)-containing oxides under near-neutral pH conditions. In acidic solutions, $Cr_2O_7^{2-}$ is the dominant $Cr(VI)_{aq}$ species, whereas in basic solutions, CrO_4^{2-} is dominant (*49*). A number of past studies have shown that Cr(VI) can be reduced to Cr(III) on such oxides via abiotic pathways (e.g., (*50-68*)). Eary and Rai (*53*) reviewed some of the most commonly used abiotic reductants and their efficiencies in reducing $Cr(VI)_{aq}$ to Cr(III) under a range of conditions in aqueous wastes. The rates of these reactions are similar to or faster than those involving biotic pathways, thus abiotic reactions could provide dominant pathways for chromate reduction (*69*). For example, Fendorf et al. (*69*) recently summarized rate data for the reduction of $Cr(VI)_{aq}$ to Cr(III) by various bacteria, organic reductants, $Fe(II)_{aq}$, and Fe(II)-containing minerals, and pointed out that magnetite has a rate similar to that of *Desulfovibrio vulgaris* (the most rapid biological reductant of $Cr(VI)_{aq}$ (*70*)). Thus, the surfaces of magnetite grains in sediments and soils can act as reductants for $Cr(VI)_{aq}$, with rates that are competitive with those of *D. vulgaris* at near-neutral pH, and maybe faster, thus more dominant, at lower pH (*69*).

Cr K-edge grazing-incidence (GI)-XAFS and Cr L-edge NEXAFS spectroscopy were used to investigate the types of surfaces complexes formed when aqueous Cr(VI) and Cr(III) at μM and mM concentrations react, respectively, with partially reduced (containing Fe^{2+}) and unreduced (containing only Fe^{3+}) single crystal (0001) hematite surfaces. Partially reduced hematite surfaces were produced by annealing hematite (0001) at ~500ºC in vacuum. Partially reduced hematite was exposed to a 5 mM Na_2CrO_4 solution (pH 6.0, 0.1 M $NaNO_3$) for 10 min. in a N_2 atmosphere, then immediately transfer-red to the UHV chamber for Cr L-edge NEXAFS data collection. Subsequently, the same sample was investigated by GI-XAFS under ambient conditions. In addition, unreduced thin-film, MBE-grown hematite(0001) was exposed to a 10^{-5} M $Cr(NO_3)_3$ solution (pH 4.8) in a N_2 atmosphere and analyzed by GI-XAFS under ambient conditions. Experimental conditions (pH, total Cr concentrations, and background electrolyte) were chosen to avoid the formation of multinuclear Cr complexes or supersaturation of Cr species in solution with respect to known hydroxides, carbonates, or basic salts (*49,71*). In addition, attempts were made to minimize the possibility of photochemical reduction of $Cr(VI)_{aq}$ during the experimental procedure. X-ray photoelectron spectroscopy was used to ensure surface cleanliness prior to the experiment and to estimate surface coverage after reaction, which is < 0.1 ML. Based on this estimated coverage and the fact that the reduced hematite (0001) surfaces have thin rafts of magnetite (111) structure (*72*), the samples examined in our GI-XAFS experiments have far less extensive reaction of $Cr(VI)_{aq}$ on the surface than the $Cr(VI)_{aq}$-reacted natural magnetite (111) samples characterized using core-level PES and L-edge absorption spectroscopy (see next section). This provides an opportunity to examine the initial stages of $Cr(VI)_{aq}$ interactions with magnetite (111) surfaces.

GI-XAFS experiments were performed at SSRL on wiggler magnet beam line 6-2, and NEXAFS experiments were performed on wiggler magnet beamline 10-1, with the

SPEAR ring operating at 3 GeV and 60-100 mA. The SSRL grazing-incidence apparatus was used to collect GI-EXAFS data in the specular geometry with the incident x-ray angle set slightly below the critical angle of the hematite substrate (≈ 0.2°). Analysis of the GI-XAFS data was performed using EXAFSPAK (*73*); k^3-weighted EXAFS were fit over a k-range of ≈ 3-11 $Å^{-1}$. Phase and amplitude functions were calculated with FEFF7 (*74*) and verified by comparison with model mineral compounds. The accuracy of the optimized parameters was estimated based on fits of crystalline model compounds (first shell: N ±15% and R ±0.03 Å; more distant shells: N ±30% and R ±0.07 Å). The Debye-Waller term ($\square^2$) for each shell was estimated based on fits of both model compounds and single-shell backtransforms and was kept fixed during the final fitting procedure. The L-edge spectrum of the Cr(VI) sorption sample (Fig. 8a) reveals features characteristic of both Cr(III) (cf. chromite) and Cr(VI) species (cf. crocoite), indicating that both Cr oxidation states are simultaneously present at the partially reduced hematite-solution interface in a ratio of ~25% Cr(III)-75% Cr(VI). The observed Cr(III) is thought to be the result of electron transfer from three Fe(II) in the partially reduced hematite to produce one Cr(III) at the hematite-aqueous solution interface.

We also carried out a Cr K-edge NEXAFS analysis of the same sample after it had been analyzed by XPS, and the result is shown in Figure 8b. The intensity of the pre-edge feature (Fig. 8b) suggests ~80% Cr(III) and ~20% Cr(VI) based

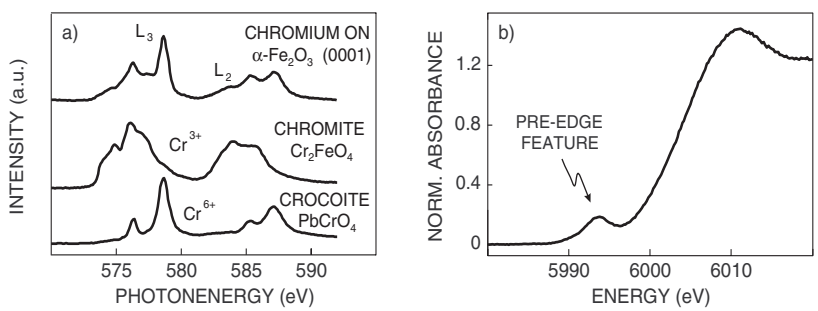

Figure 8. a) Normalized Cr L-edge NEXAS spectra of a Cr(VI)-exposed, partially reduced hematite sample compared to Cr(VI) and Cr(III) model compounds, b) Corresponding Cr K-edge NEXAFS spectrum. From (75).

on the calibration spectra of Peterson et al. (*63*). The apparent difference between these two experiments is most likely due to further reduction of Cr(VI) on the partially reduced hematite (0001) surface during XPS analysis, which involved the use of a low energy electron flood gun to charge neutralize the surface. Thus the Cr(VI):Cr(III) ratio from the L-edge spectrum is more reliable for this Cr(VI)/hematite sorption sample. The simultaneous presence of both oxidation states at the interface, even after extended exposure times, points to a limited reducing capacity of the partially reduced hematite which is depleted during the course of the experiment.

Figure 9 shows the GI-EXAFS spectra and resulting Fourier transform (FT) of an unreduced hematite (0001) surface exposed to a Cr(III)-containing solution (Fig. 9, top) in comparison with a partially reduced sample exposed to $Cr(VI)_{aq}$ (Fig. 9, bottom). Despite the different reaction pathways, the least-squares fitting results in a similar local

structure of the observed Cr surface species for both samples. The first feature in the FT is due to Cr-O correlations while the second FT feature is most likely due to Cr-Cr correlations (see discussion below). In addition, there is evidence for a more distant (~3.5 Å) metal-metal shell (Cr-Fe or Cr-Cr), which, however, is difficult to resolve unambiguously. This third shell is best fit by a Cr-Fe correlation, and could be evidence for direct bonding of Cr(III) to the hematite surface in a tridentate fashion. It is important to note that the GI-XAFS spectra taken with the E-vector parallel to the hematite surface should be particularly sensitive to Cr-metal correlations parallel to the hematite surface, and much less sensitive to Cr-metal correlations perpendicular to the surface. GI-XAFS spectra taken with the E-vector perpendicular to the hematite (0001) surface are needed to confirm the presence of Cr-$Fe_{surface}$ correlations. None of the hypothetical surface complexes representing monomer adsorption is consistent with the local structure obtained in the GI-XAFS analysis (*75*). Consequently, we propose a multinuclear surface complex rather than a mononuclear complex, which is often assumed in surface complexation modeling (e.g., (*76*)). The observed metal-metal distance of ~3.0 Å is consistent with edge-sharing metal-oxygen (MeO_6) octahedra with either Fe or Cr as the central metal atom (*77*). Even though the fitted number of second-shell metal neighbors is approximately two, suggesting that the Cr-metal clusters are fairly limited in size or are arranged in a disordered fashion. The lack of more pronounced next-nearest neighbor metal shell features is consistent with this finding and further emphasizes the limited size of the proposed "two-dimensional" multinuclear species on partially reduced hematite (0001).

The different metal backscatterer correlations cannot be identified unambiguously due to the similarity of the Cr and Fe phase shift and amplitude functions, respectively. Nevertheless, the GI-XAFS information obtained regarding the local structure of the Cr species provides relatively restrictive geometrical constraints due to the polarized nature of the spectra. Multinuclear Cr complexes, in particular dimers and trimers sorbed in a two-dimensional fashion to the atomically flat hematite (0001) surface, are consistent with the observed spectra. The more distant metal-metal shell at 3.5 Å is consistent with Fe backscatterers from the hematite (0001) surface arranged in a somewhat disordered fashion. In this case, the Cr-Fe bonds would have a significant component in the E-vector parallel spectra. In addition, evidence for a true Cr(III) sorption complexes on the surface of reduced hematite comes from a consideration of solution conditions, which do not favor multinuclear species or precipitates [see (*75*)].

The existence of Cr at the hematite-water interface in multinuclear complexes even at a surface coverage of < 0.1 monolayer was not anticipated based on the findings of earlier EXAFS studies of metal ion surface complexation as a function of metal loading. For example, the EXAFS studies of Chisholm-Brause et al. (*78*) and Towle et al. (*79,80*) found evidence for mononuclear complexes of Co(II) on alumina at the lowest surface coverages examined (~0.05 $\mu M/m^2$), with multinuclear complexes or precipitates forming at higher surface coverages. Nevertheless, our suggestion of multinuclear Cr(III) surface complexes is consistent with observations elaborated in previous studies involving Cr(III) sorption on iron oxides (*77,81*).

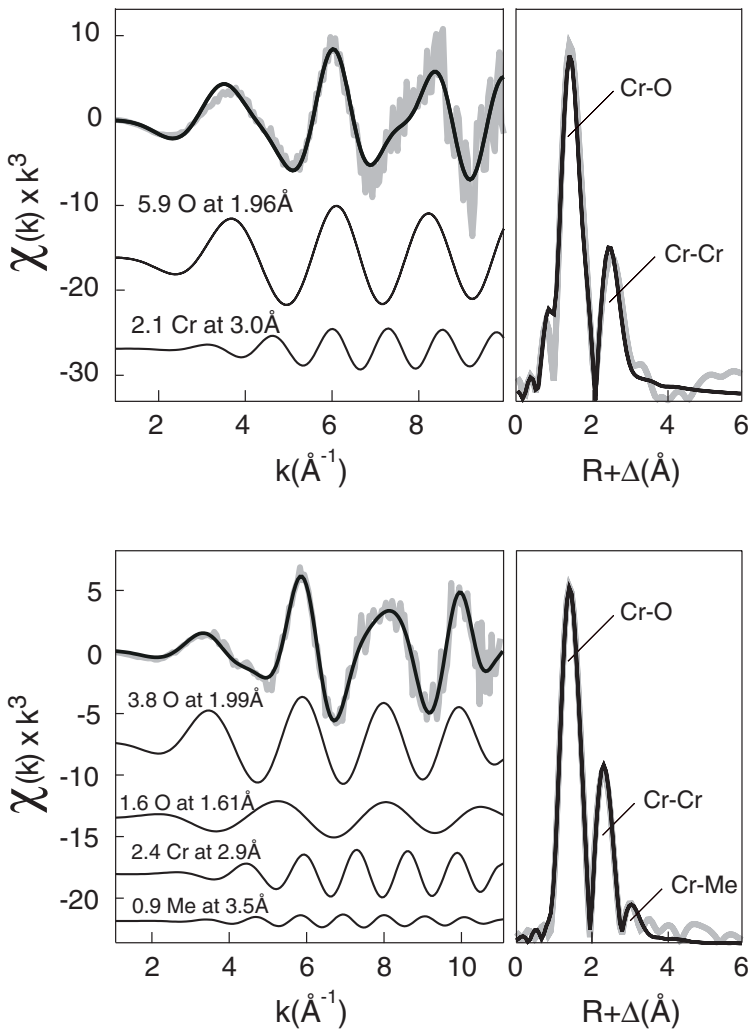

Figure 9. Grazing-incidence Cr K-edge XAFS data (gray) of chromium sorbed on α-Fe_2O_3 single crystals (0001). Top: Unreduced hematite (0001) reacted with $Cr(III)_{aq}$. Bottom: Partially reduced hematite (0001) exposed to $Cr(VI)_{aq}$. Least squares fits of the EXAFS including shell-by-shell deconvolution and Fourier transforms (uncorrected for phase shift) are shown. From (75).

F. The Nature of the Reacted Layer and Kinetics of $Cr(VI)_{aq}$ Reduction Reaction on Magnetite Surfaces

The grazing-incidence XAFS study of $Cr(VI)_{aq}$ sorption on reduced hematite (0001) surfaces discussed above provided information about the structure, composition, and mode of attachment of Cr(III) sorption complexes on this surface at submonolayer Cr surface coverages. To obtain quantitative information about the composition, structure, and thickness of the overlayer produced by the reaction of $Cr(VI)_{aq}$ with magnetite, we used a combination of soft x-ray core-level photoemission and adsorption spectroscopies (*82*). Samples were prepared by reacting 50 μM aqueous Na_2CrO_4 solutions at pH 6 and 8.5 with clean surfaces of magnetite(111) prepared under UHV conditions. The spectra were measured on beam line 10-1 at SSRL. Chromium 2p photoemission and Cr L-edge

absorption (Fig. 10) show that tetrahedrally coordinated $Cr(VI)_{aq}$ is reduced by a heterogeneous redox process to octahedral Cr(III) on the magnetite (111) surface. The thickness of the reacted overlayer at pH 6 was found to increase with immersion time in the chromate solution for up to ≈ 10 min. and to remain unchanged for longer doses. The reaction rate at pH 6 was found to be initially fast and to follow a logarithmic law (Fig. 11). At saturation, the passivating overlayer is 15±5 Å thick and consists of chromium (oxy)hydroxide with only trace amounts of iron.

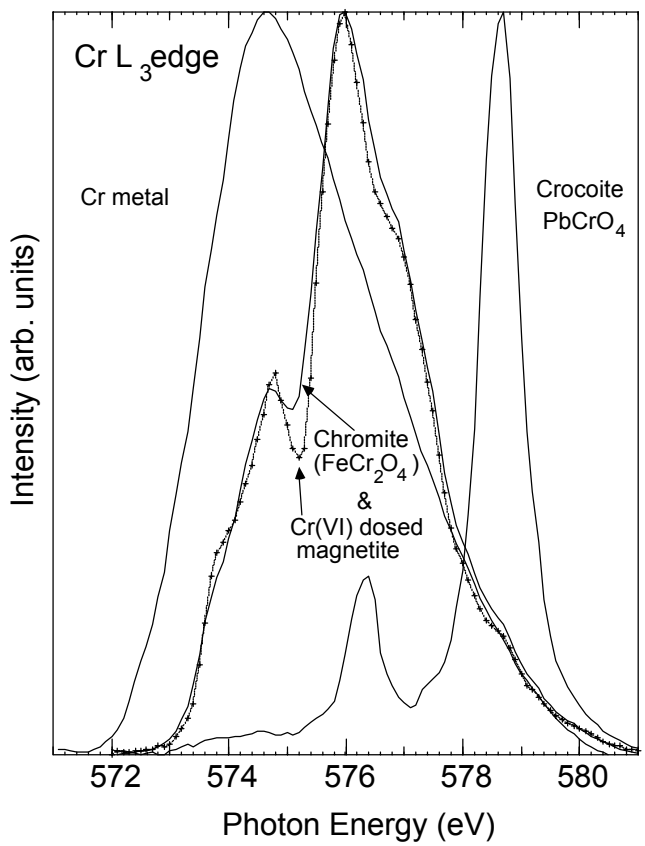

Figure 10. Cr L_3-edges of $Cr(VI)_{aq}$-reacted magnetite (111) compared with the Cr L_3-edges of Cr metal, chromite, and crocoite. From (82).

Evidence for extensive hydroxylation in the overlayer was provided by a chemically shifted component in the O 1s photoemission (Fig. 12) and O K-edge absorption spectra taken with surface-sensitive O KVV Auger yield (feature A in Fig. 13). The overlayer appears to lack long-range order based on loss of the first EXAFS-like feature in the O K-edge spectrum with increasing dosing time (feature B in Fig. 13). Clear evidence for oxidation of Fe(II) to Fe(III) in the surface region of the magnetite substrate during reduction of $Cr(VI)_{aq}$ to Cr(III) was provided by Fe 2p photoemission and Fe L-edge absorption spectra (not shown). Strong attenuation of the Fe 2p signal during the first 10 minutes of the redox reaction indicated that iron does not outdiffuse to the overlayer. At pH 8.5 the reaction follows a similar path, but its rate is slower and Cr(VI) reduction continues for immersion times of up to one hour (Fig. 11). This difference is due in part

to the lower affinity of the CrO_4^{2-} and $Cr_2O_7^{2-}$oxoanions at pH 8.5 vs. pH 6 due to the fact that the magnetite surface is negatively charged at pH values above its point of zero charge, 6.6 (*83*), and positively charged below the pH_{pzc}.

The results of this study compare well with those from an earlier XPS study of the passivation of "zero-valent" iron by Cr(VI)-containing solutions (*84*). The resulting overlayer compositions, thicknesses, and reaction rates are very similar for the two systems. Once the magnetite or "zero-valent" iron surface is passivated by a relatively thin layer of disordered Cr-(oxy)hydroxide, the electron transfer reaction responsible for the reduction of $Cr(VI)_{aq}$ should stop.

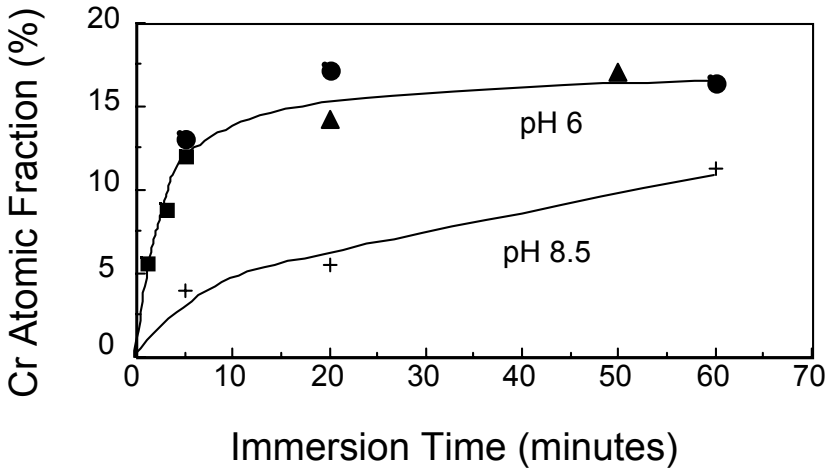

Figure 11. Atomic fraction of Cr for the overlayers studied plotted as a function of immersion time in 50 µM sodium chromate solutions at pH 6 and pH 8.5. These results were obtained from the intensities of the Cr 2p, Fe 2p, and O 1s core levels. From ***(82)****.*

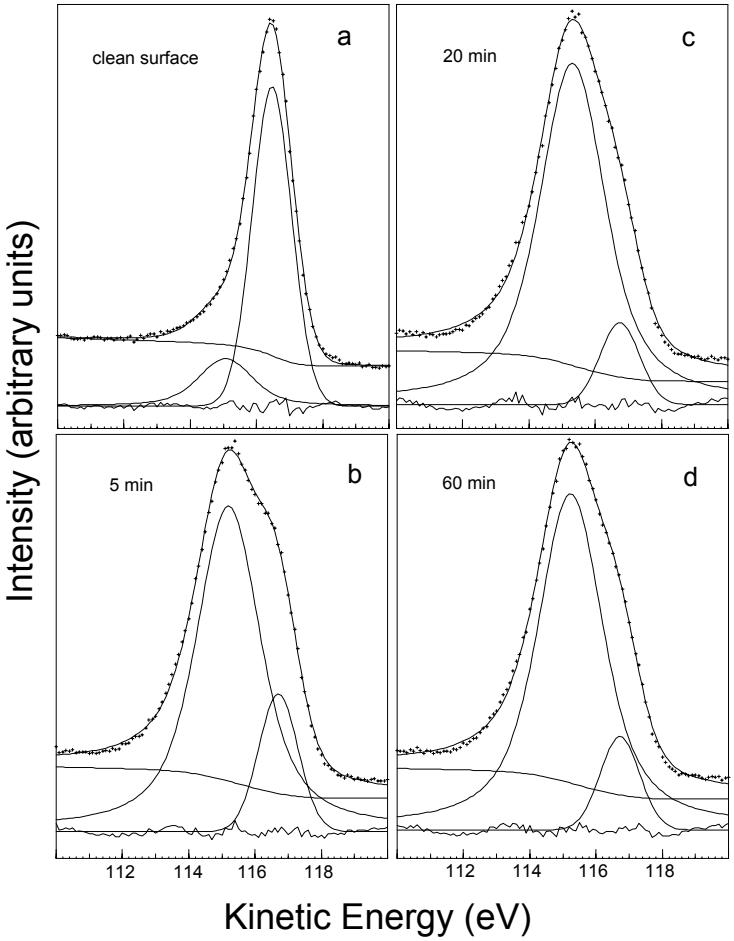

Figure 12. Oxygen 1s photoemission spectra of a $Cr(VI)_{aq}$-reacted magnetite (111) sample as a function of dosing time. From ***(82)****.*

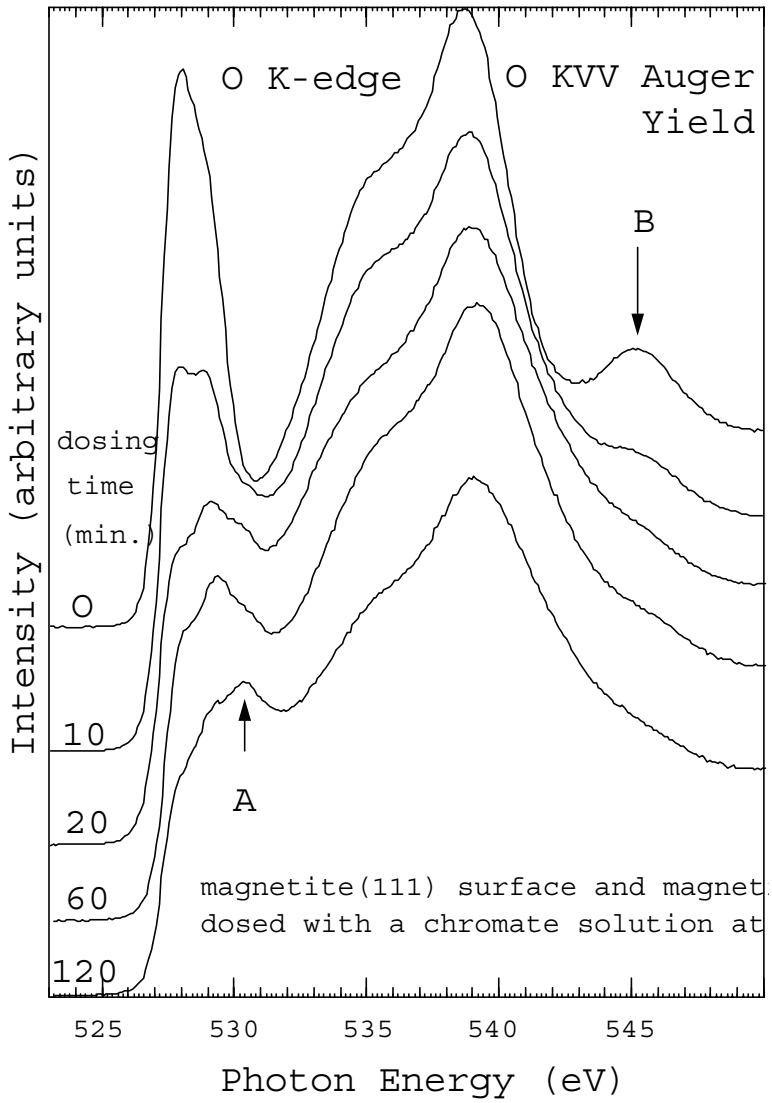

*Figure 13. Oxygen K-edge x-ray absorption spectra of $Cr(VI)_{aq}$-reacted magnetite(111) as a function of dosing time (in minutes). From **(82)**.*

G. $Cr(VI)_{aq}$ Sorption on Hematite Surfaces in the Presence of Phosphate and Sulfate

Powdered hematites present several crystalline faces for surface reactions and thus represent a system that is intermediate in complexity between the single-crystal surfaces described above and the heterogeneous mixture of surfaces found in soils and sediments. We conducted several experiments with hematite powder to understand the thermodynamics and kinetics of $Cr(VI)_{aq}$ sorption, with particular emphasis placed on competitive sorption by $Cr(VI)_{aq}$, phosphate, and sulfate oxoanions.

Batch sorption experiments with 20 mg of hematite powder (specific surface of 9.7 m^2g^{-1} by BET-N_2) in a 15 mL solution were conducted at room temperature with initial chromate, phosphate, or sulfate concentrations ranging from 2.7 to 54 μM (i.e., 140

ppb to 2.8 ppm). Preliminary experiments established that equilibration times of one hour were sufficient, and the concentrations of the anions remaining in solution after this time were determined by ion chromatography. The solutions were not buffered for pH to eliminate interferences from the anions associated with buffering agents, and as a consequence, final sorption pH's ranged from 6.0 to 6.8. Despite the range in final pH, the results of these sorption experiments (Fig. 14) could be described well by the linearized Langmuir isotherm equation:

$$C_{final}/C_{sorbed} = (1/C_{max})C_{final} + 1/(K_{ads}\ C_{max})$$

where C_{final} and C_{sorbed} are the equilibrium concentrations in solution and on the hematite surface, respectively, C_{max} is the maximum sorption capacity of the mineral under the conditions of the experiment, and K_{ads} is the Langmuir adsorption constant.

Values for K_{ads}, which is a surface-complexation constant and thus a measure of the specific binding affinity of a surface site for the anion, were 0.27,

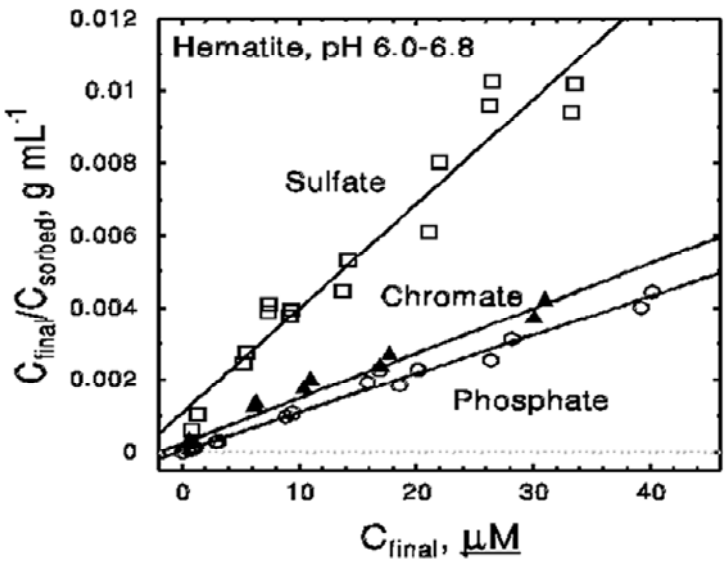

Figure 14. Linearized Langmuir isotherm plots of sorption of mono-anionic solutions of sulfate, $Cr(VI)_{aq}$, and phosphate on hematite powder.

0.25, and 2.4 for sulfate, $Cr(VI)_{aq}$, and phosphate, respectively. These results can be interpreted as suggesting an outer-sphere (i.e., hydrated anion) binding mechanism for sulfate and $Cr(VI)_{aq}$, and an inner-sphere mechanism for phosphate. Maximum sorption capacities of the hematite for sulfate, $Cr(VI)_{aq}$, and phosphate were 3.5, 8.3, and 9.3 µmol g^{-1}, respectively, indicating that more sorption sites for $Cr(VI)_{aq}$ and phosphate were available than for sulfate. The low C_{max} values for sulfate could be related to the absence of a protonated species, and suggest that hydrogen bonding of $Cr(VI)_{aq}$ and phosphate to neutral oxygen surface sites could increase the total number of sites available for sorption of these anions. In fact, C_{max} is strongly correlated with pK_2, the negative log of the second acid dissociation constant for each anion (Fig. 15).

For competitive sorption between these anions, however, other factors such as aqueous speciation must also be considered. Simple electrostatic considerations suggest that divalent anionic species will be more strongly attracted to positively charged surface sites than monovalent species. When both types of species are present in solution and in excess of the available surface sites, divalent species species (i.e., SO_4^{2-}, CrO_4^{2-}, $Cr_2O_7^{2-}$, and HPO_4^{2-}) should dominate the observed sorption behavior. This premise can be tested by competitive sorption experiments because the amounts of divalent anion available for sorption will vary differently for each anion when pH's close to the

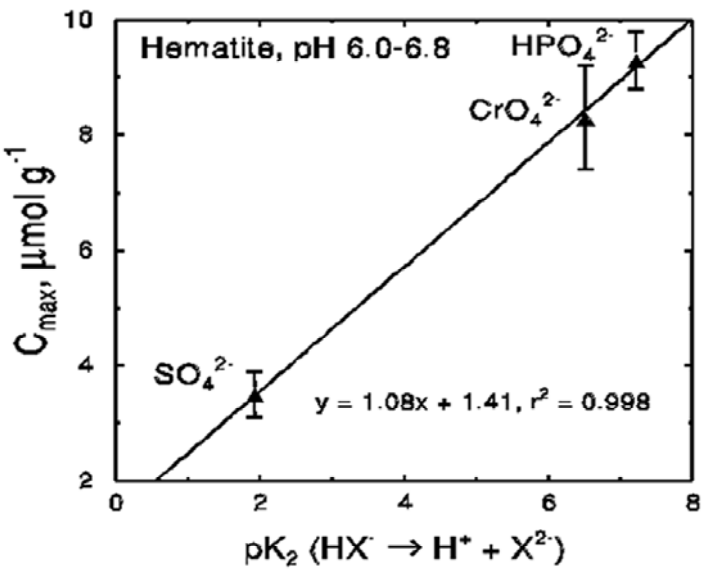

Figure 15. Correlation between observed C_{max} values for sorption by mono-anionic solutions of sulfate, $Cr(VI)_{aq}$, and phosphate on hematite powder and the acidities of the anions.

pK_2 values are selected. Although experiments at pH's near the pK_2 of sulfate are impractical, such experiments with $Cr(VI)_{aq}$ and phosphate are both practical and directly relevant to groundwater chemistry because the pK_2 values for these anions are near 7.

The expectation is that the relative sorption of $Cr(VI)_{aq}$ and phosphate would be directly proportional to the aqueous concentrations of $Cr(VI)_{aq}$ and HPO_4^{2-}. Speciation calculations show that the ratio of these two species in solution (i.e., HPO_4^{2-}/ $Cr(VI)_{aq}$) varies from about 0.2 to 1 in going from pH 4 to 9 (Fig. 16, solid curve) and suggest that sorption of $Cr(VI)_{aq}$ would be favored over phosphate over much of this range. The linear relationship between C_{max} and pK_2 suggests that the relative numbers of available sites for $Cr(VI)_{aq}$ and HPO_4^{2-} are constant regardless of pH, provided that the same sorption mechanisms are involved. Combining the speciation and site-availability data, we can estimate the relative amount of total phosphate needed to achieve 50% sorption [i.e., equivalent sorption with $Cr(VI)_{aq}$] by

$$[P_{total}/Cr(VI)_{total}]50\% = [C_{max}(Cr(VI))/C_{max}(P)][CrO_4^{2-}/HPO_4^{2-}].$$

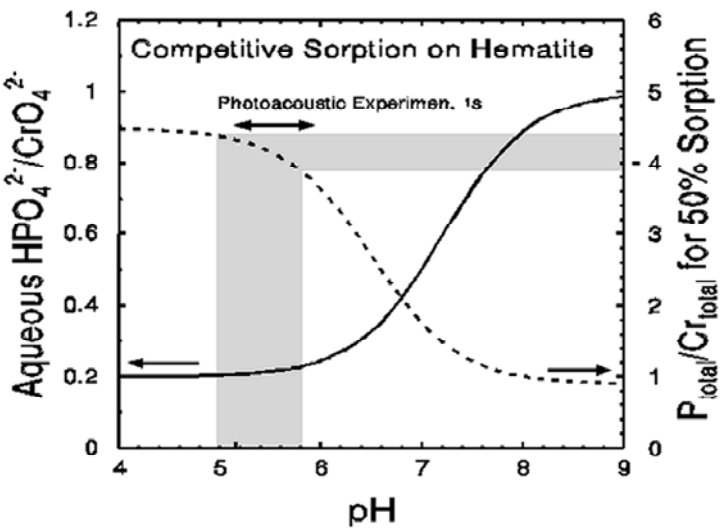

Figure 16. Influence of pH on aqueous speciation of phosphate and $Cr(VI)_{aq}$ (solid line-left axis) and the predicted ratio of total phosphate to $Cr(VI)_{aq}$ needed to achieve equal sorption on hematite powder (dashed line-right axis).

This result is also plotted in Figure 16 (dotted curve, right axis). On this basis, we would predict that about 4.4 times as much phosphate as $Cr(VI)_{aq}$ would be needed at pH 5 for equal sorption by the two anions on powdered hematite, whereas at pH 8 the same concentration of phosphate as $Cr(VI)_{aq}$ would yield equal sorption. The prediction at pH 5 is in reasonable agreement with the results of competitive sorption experiments carried out at low ionic strength using laser photoacoustic spectroscopy (LPAS, shown by the shaded portion of the graph). Experiments carried out at pH 5 (±0.1) in 10 mM KCl to minimize pH drift, however, routinely require ratios of phosphate to $Cr(VI)_{aq}$ near 7 for equivalent sorption to occur. A 40-fold excess of phosphate completely inhibits $Cr(VI)_{aq}$ sorption under these conditions.

The competitive sorption results are different when the phosphate contacts the hematite after the $Cr(VI)_{aq}$ has reacted with it. A delay in phosphate addition results in incomplete desorption of Cr(VI). Between 25 and 50% of the Cr(VI) seems irreversibly bound to the hematite if 15-30 minutes elapse between initial sorption and the addition of phosphate. This result suggests substantial alteration or reorganization of the Cr(VI) once sorbed. Examples of the types of mechanisms that could be responsible for this behavior include conversion from monodentate to bidentate sorption, coalescence/polymerization of isolated chromate ions on the surface, or conversion from outer- to inner-sphere bonding.

Using the same approach as just outlined for phosphate to predict competitive sorption between sulfate and $Cr(VI)_{aq}$ suggests that at pH 5, a $S_{total}/Cr(VI)_{total}$ ratio of about 0.07 is sufficient to achieve 50% sorption, largely because at this pH only about 3% of the Cr(VI) is in the form of CrO_4^{2-}, whereas all the sulfate is divalent. Experimental verification of this prediction, however, shows that a $S_{total}/Cr(VI)_{total}$ ratio of about 500 is required for equivalent sorption of $Cr(VI)_{aq}$ and sulfate. Clearly, different

mechanisms are involved in sorption of $Cr(VI)_{aq}$ and sulfate, the most likely difference being a different suite of available sorption sites and the possible stabilizing behavior from hydrogen bonding of Cr(VI) and surface oxygens. Delayed addition of sulfate after $Cr(VI)_{aq}$ /hematite reaction yielded results similar to those for phosphate.

Based on these results, which will be reported in detail elsewhere (*85*), we can draw the following conclusions. Sorption of $Cr(VI)_{aq}$ and phosphate species on hematite is dominated by divalent anions even at low pH's where monovalent anions predominate in solution. As a consequence, aqueous speciation (i.e., the fraction of the total species in solution available in the form of divalent anions) is a more important determinant of the relative amount of $Cr(VI)_{aq}$ or phosphate sorbed than the intrinsic selectivity of the anions for the surface. Although completely divalent, sulfate is not very competitive with $Cr(VI)_{aq}$ for sorption sites on hematite, probably as the result of their preference for different types of sorption sites and the potential for hydrogen bonding with $Cr(VI)_{aq}$ species. Delayed addition of phosphate or sulfate after initial $Cr(VI)_{aq}$ sorption, however, shows that some type of rearrangement of the Cr(VI)-surface bond occurs in the first 15-30 minutes after sorption, which renders a large fraction of the Cr(VI) tightly bound to the surface. In mixed-anion systems typical of groundwater, significantly different sorption affinities may be observed than predicted solely on the basis of relative single-anion sorption constants.

An important outcome of this work is the development of a powerful new tool with which competitive adsorption of anions on minerals in suspension can be investigated in real time. We have demonstrated that nontoxic anions present in the subsurface environment, such as phosphate, may compete with toxic anions, such as $Cr(VI)_{aq}$, for sorption sites on redox-active minerals to an extent that is highly pH dependent. Significantly, LPAS can be used for studies of pure mineral phases, such as hematite in the present experiments, as well as for multi-component soil mixtures. Thus, controlled and "real-world" experiments can be carried out to determine the extent to which competing nontoxic anions can prevent adsorption and reduction of toxic anions by minerals or redox-active remediation agents, such as "zero-valent" iron.

IV. Conclusions

The following conclusions can be drawn from our study of the interaction of $Cr(VI)_{aq}$ with magnetite and reduced hematite surfaces:

1. Metal oxide-aqueous solution interfaces are extremely complex and poorly understood at the molecular level. Spectroscopic and molecular modeling studies of the reaction of aqueous sorbates with well-characterized, single crystal, metal oxide surfaces can provide some of this understanding.
2. Oxygen-plasma-assisted MBE permits the growth of iron oxides with well-defined stoichiometries and crystal orientations for use in studies of the interaction of water and $Cr(VI)_{aq}$ with iron oxides.
3. The geometric and electronic structures of clean iron oxide surfaces are better understood than the water-exposed surfaces. In both cases, significant but different reconstructions occur. The structure of the vacuum-iron oxide interface is different from that of the solution-iron oxide interface.

4. Water dissociates and chemisorbs on iron oxide surfaces at ambient temperature, initially on defect sites, then at a threshold $p(H_2O) > 10^{-4}$ torr on terrace sites, resulting in ≈ 0.5 ML of hydroxyls. At $p(H_2O) \geq 10^{-2}$ torr, ≈ 1 ML of hydroxyls is found on hematite (0001) and magnetite (111).
5. XAFS and photoemission spectroscopies clearly show that $Cr(VI)_{aq}$ is reduced to Cr(III) on hydrated iron oxide surfaces that contain Fe^{2+}, but not on hydrated surfaces that contain only Fe^{3+}.
6. Cr and Fe L-edge XAFS and Cr 2p and Fe 2p photoemission spectroscopy show that the magnetite surface is quickly passivated, and the Cr(VI)→Cr(III) reduction reaction ceases after the formation of an electrically insulating layer of 15±5 Å in thickness. This finding has major implications for the use of magnetite, other Fe(II)-containing solids, or "zero-valent" iron for remediating $Cr(VI)_{aq}$-contaminated groundwater.
7. The passivating layer on magnetite consists initially of a poorly crystalline Cr-(oxy)hydroxide phase on a thin Fe(III)-oxide substrate. Comparison of Cr 2p, Fe 2p, and O 1s photoemission data for $Cr(VI)_{aq}$-reacted magnetite (this study) and "zero-valent" iron (*84*) suggests that similar phases form on "zero-valent" iron after reaction with $Cr(VI)_{aq}$.
8. The Cr(VI)→Cr(III) reduction reaction goes to completion on hyrdrated magnetite surfaces in ≈ 10 minutes at pH 6.0 and within ≈ 1 hour at pH 8.5, the difference being related to the higher affinity of CrO_4^{2-} and $Cr_2O_7^{2-}$oxoanions for the magnetite surface below its point of zero charge (pH 6.6), where it is positively charged.
9. Common soil anions have some potential to interfere with $Cr(VI)_{aq}$ uptake on iron oxides in soils and sediments. Photoacoustic spectroscopy and batch adsorption isotherm measurements indicate the following:
   - Sulfate does not interfere significantly with $Cr(VI)_{aq}$ sorption on iron oxides until present in 500-fold excess.
   - Phosphate species requires a 4- to 7-fold excess to interfere significantly with $Cr(VI)_{aq}$ sorption below pH 6, but will interfere at equal concentrations above pH 7.
10. The fraction of total species in solution available in the form of divalent anions is a more important determinant of the relative amount of $Cr(VI)_{aq}$ or phosphate sorbed on iron oxides than the intrinsic selectivity of the anions for the surface.
11. Sorbed Cr(VI) species are much more difficult to remove by competing anions when these anions are added after $Cr(VI)_{aq}$ has reacted with hematite than if they are added concurrently with $Cr(VI)_{aq}$.

V. Appendices

A. References (including all papers published under the auspices of this program)

1. Greenwood, N.N.; Earnshaw, A. *Chemistry of the Elements*. Pergammon Press, Oxford, U.K., 1984.
2. Richard, F.C.; Bourg, A.C.M. *Water Res.* **1991**, *25*, 807.
3. Gauglhofer, J.; Bianchi, V. In: *Metals and Their Compounds in the Environment*, E. Merian, ed., VCH, Weinheim, Germany, 1991.
4. Gao, Y.; Kim, Y.J.; Chambers, S.A.; Bai, G. *J. Vac. Sci. Technol*. **1997**, *A15*, 332.
5. Yi, S.I.; Liang, Y.; Chambers, S.A. *J. Vac. Sci. Technol*., **1999**, *A17*, 1737.
6. Thevuthasan, S.; Kim, Y.J.; Yi, S.I.; Chambers, S.A.; Morais, J.; Denecke, R.; Fadley, C.S.; Liu, P.; Kendelewicz, T.; Brown, G.E., Jr., *Surf. Sci.* **1999**, *425*, 276.
7. Chambers, S.A.; Kim, Y.J.; Gao, Y. *Surf. Sci. Spectra* **1998**, *5*, 219.
8. Kim, Y.J.; Gao, Y.; Chambers, S.A. *Surf. Sci.* **1997**, *371*, 358.
9. Yi, S.I.; Liang, Y.; Chambers, S.A. *Surf. Sci.* **1999**, *443*, 212.
10. Gao, Y.; Chambers, S.A. *J. Cryst. Growth* **1999**, *174*, 446.
11. Chambers, S.A.; Joyce, S.A. *Surf. Sci*. **1999**, *420*, 111.
12. Gao, Y.; Kim, Y.J.; Chambers, S.A. *J. Mater. Res.* **1998**, *13*, 2003.
13. Gao, Y.; Kim, Y.J.; Thevuthasan, S.; Chambers, S.A.; Lubitz, P. *J. Appl. Phys*. **1997**, *81*, 3253.
14. Yi, S.I.; Liang, Y.; Thevuthasan, S.; Chambers, S.A. unpublished.
15. Chambers, S.A.; Yi, S.I. *Surf. Sci*. **1999**, *439*, L785.
16. Wang, X.-G.; Weiss, W.; Shaikhutdinov, S.K.; Ritter, M.; Peterson, M.; Wagner, F.; Schlogl, R.; Scheffler, M. *Phys. Rev. Lett.* **1998**, *81*, 1038.
17. Shaikhutdinov S.K.; Weiss, W. *Surf. Sci*. **1999**, *432*, L627.
18. Bloemen, P.J.H.; van der Heijden, P.A.A.; Wolf, R.M.; aan de Stegge, J.; Kohlhepp, J.T.; Reinders, A.; Jungblut, R.M.; van der Zaag, P.J.; de Jonge, W.J.M. *Mater. Res. Soc. Symp. Proc.* **1996**, *401*, 485.
19. Anderson, J.F.; Kuhn, M.; Diebold, U.; Shaw, K.; Stroyanov, P.; Lind, D. *Mater. Res. Soc. Symp. Proc*. **1997**, *474*, 265.
20. Gaines, J.M.; Kohlhepp, J.T.; Van Eemeren, J.T.W.M.; Elfrink, R.J.G.; Roozeboom, F.; De Jonge, W.J.M. *Mater. Res. Soc. Symp. Proc*. **1997**, *474*, 191.
21. Gaines, J.M.; Bloemen, P.J.H.; Kohlhepp, J.T.; Bulle-Lieuwma, C.W.T.; Wolf, R.M.; Reinders, A.; Jungblut, R.M., van der Heijden, P.A.A.; van Eemeren, J.T.W.M.; aan de Stegge, J.; de Jonge, W.J.M. *Surf. Sci.* **1997**, *373*, 85.
22. Gaines, J.M.; Kohlhepp, J.T.; Bloemen, P.J.H.; Wolf, R.M.; Reinders, A.; Jungblut, R.M. *J. Magn. Magn. Mater*. **1997**, *165*, 439.
23. The specimen was transferred from the MBE chamber at PNNL to an STM chamber down the hall through air in ~10 minutes. For a complete description of the experiment, see Chambers, S.A.; Thevuthasan, S.; Joyce, S.A. *Surf. Sci.* **2000** (in press).
24. The specimen was transferred from the MBE chamber at PNNL to an evacuated shipping container through air, and then from the shipping container to the STM chamber at Tulane again through air. The total time in air was ~90 minutes. For a

complete description of the experiment, see Stanka, B.; Hebenstreit, W.; Diebold, U.; Chambers, S.A. *Surf. Sci*. **2000**, *448*, 49.
25. Terrach, G.; Burgler, D.; Schaub, T.; Wiesendanger, R.; Guntherodt, H.-J. *Surf. Sci*. **1993**, *285*, 1.
26. Voogt, F.C. Ph.D. thesis, Departments of Chemical Physics and Nuclear Solid State Physics, University of Groningen, The Netherlands, 1998.
27. Kendelewicz, T.; Liu, P.; Doyle, C.S.; Brown, G.E., Jr.; Nelson, E.J.; Chambers, S.A. *Surf. Sci*. **2000**, (in press).
28. Liu, P.; Kendelewicz, T.; Brown, G.E. Jr.; Nelson, E.J.; Chambers, S.A. *Surf. Sci.* **1998**, *417*, 53-65.
29. Liu, P.; Kendelewicz, T.; Brown, G.E., Jr.; Parks, G.A. *Surf. Sci.* **1998**, *412/413*, 287.
30. Liu, P.; Kendelewicz, T.; Brown, G.E., Jr. *Surf. Sci.* **1998**, *412/413*, 315.
31. Giordano, L.; Goniakowski, J.; Suzanne, J. *Phys. Rev. Lett*. **1998**, *81*, 1271.
32. Hass, K.C.; Schneider, W.F.; Curioni, A.; Andreoni, W. *Science* **1998**, *282*, 265.
33. Halley, J.W.; Rustad, J.R.; Rahman, A. *J. Chem. Phys.* **1993**, *98*, 4110.
34. Stillinger F.H.; David, C.W. *J. Chem. Phys*. **1978**, *69*, 1473.
35. Curtiss, L.A.; Halley, J.W.; Hautman, J.; Rahman, A. *J. Chem. Phys*. **1987**, *86*, 2319.
36. Rustad, J.R.; Hay, B.P.; Halley, J.W. *J. Chem. Phys*. **1995**, *102*, 427.
37. Rustad, J.R.; Felmy, A.R.; Hay, B.P. *Geochim. Cosmochim. Acta* **1996**, *60*, 1553.
38. Wasserman, E.; Rustad, J.R.; Hay, B.P.; Halley, J.W. *Surf. Sci.* **1997**, *385*, 217.
39. Henderson, M.A.; Joyce, S.A.; Rustad, J.R. *Surf. Sci*. **1998**, *417*, 66.
40. Rustad, J.R.; Wasserman, E.; Felmy, A.R. *Surf. Sci*. **1999**, *424*, 28.
41. Rustad, J.R.; Felmy, A.R.; Hay, B.P. *Geochim. Cosmochim. Act*a **1996**, *60*, 1563.
42. Felmy, A.R.; Rustad, J.R. *Geochim. Cosmochim. Acta* **1998**, *62*, 25.
43. Wang, X.-G.; Weiss, W.; Shaikhutdinov, S.K.; Ritter, M.; Petersen, M.; Wagner, F.; Schlogl, R.; Scheffler, M. *Phys. Rev. Lett*. **1998**, *81*, 1038.
44. Rustad, J.R.; Wasserman, E.; Felmy, A.R. *Surf. Sci*. **1999**, *432*, L583.
45. Akesson, R.; Pettersson, L.G.M.; Sandstrom, M.; Wahlgren, U. *J. Am. Chem. Soc.* **1994**, *116*, 8691.
46. Rustad, J.R.; Wasserman, E.; Felmy, A.R. *Proc. 2nd Internat. Alloy Conf.*, Davos, Eds. Gonis, A.; Meike, A.; Turchi, P.E.A. **2000** (in press).
47. Stanka, B.; Hebenstreit, W.; Diebold, U.; Chambers, S.A. *Surf. Sci.* **2000**, *448*, 49.
48. Hamilton, W.C. *Phys. Rev.* **1958**, *110*, 1050.
49. Baes F.B.; Mesmer, R.E. *The Hydrolysis of Cations*. Krieger Publishing Co., Malabar, Florida, 1996.
50. Mayer, L.M.; Schick, L.L. *Environ. Sci. Technol*. **1981**, *15*, 1482.
51. James, B.R.; Bartlett, R.J. *J. Environ. Qual.* **1983**, *12*, 177.
52. Music', S.; Ristic, M.; Tonkovic, M. *Z. Wasser-Abwasser-Forsch.* **1986**, *19*, 186.
53. Eary, L.E.; Rai, D. *Environ. Sci. Technol.* **1988**, *22*, 972.
54. Eary, L.E.; Rai, D. *Am. J. Sci.* **1989**, *289*, 180.
55. Eary, L.E.; Rai, D. *Soil Sci. Soc. Am. J.* **1991**, *55*, 676.
56. Eckert, J.M.; Stewart, J.J.; Waite, T.D.; Szymczak, R.; Williams, K.L. *Anal. Chim. Acta* **1990**, *236*, 357.
57. Bidoglio, G.; Gibson, P.N.; O'Gorman, M.; Roberts, K.J. *Geochim. Cosmochim. Acta* **1993**, *57*, 2389.
58. Anderson, L.D.; Kent, D.B.; Davis, J.A. *Environ. Sci. Technol.* **1994**, *28*, 178.

59. Weng, C.H.; Huang, C.P.; Allen, H.E.; Cheng, A.H-D.; Sanders, P.F. *Sci. Total. Environ.* **1994**, *154*, 71.
60. Weckhuysen, B.M.; Wachs, I.E.; Schoonheydt, R.A. *Chem. Rev.* **1996**, *96*, 3327.
61. Fendorf, S.E.; Li, G. *Environ. Sci. Technol.* **1996**, *30*, 1614.
62. White, A.F.; Peterson, M.L. *Geochim. Cosmochim. Acta* **1996**, *60*, 3799.
63. Peterson, M.L.; Brown, G.E., Jr.; Parks, G.A. *Colloids Surf. A* **1996**, *107*, 77.
64. Peterson, M.L.; White, A.F.; Brown, G.E., Jr.; Parks, G.A. *Environ. Sci. Technol.* **1997**, *31*, 1573.
65. Peterson, M.L.; Brown, G.E., Jr.; Parks, G.A.; Stein, C.L. *Geochim. Cosmochim. Acta* **1997**, *61*, 3399.
66. Patterson, R.R.; Fendorf, S.; Fendorf, M. *Environ. Sci. Technol.* **1997**, *31*, 2039.
67. Szulczewski, M.D.; Helmke, P.A.; Bleam, W.F. *Environ. Sci. Technol.* **1997**, *31*, 2954.
68. Jardine, P.M.; Fendorf, S.E.; Mayers, M.A.; Larsen, I.L.; Brooks, S.C.; Bailey, W.B. *Environ. Sci. Technol.* **1999**, *33*, 2939.
69. Fendorf, S.E.; Wielinga, B.W.; Hansel, C.M. *Geol. Internat.* 2000 (in press).
70. Lovley, D.R.; Phillips, E.J.P. *Appl. Environ. Microbiol.* **1994**, *60*, 726.
71. Smith, R.M.; Martell, A.E. *Critical Stability Constants*. Plenum Press, New York, 1976.
72. Condon, N.G.; Murray, P.W.; Leibsle, F.M.; Thornton, G.; Lennie, A.R.; Vaughan, D.J. *Surf. Sci.* **1994**, *310*, L609.
73. George, G.N.; Pickering, I.J. *EXAFS-PAK*. Technical Report, Stanford Synchrotron Radiation Laboratory, Stanford, CA, 1995.
74. Ankudinov, A.L.; Ravel B.; Rehr, J.J.; Conradson, S.D. *Phys. Rev□□□. B* **1998**, *58*, 7565□□.
75. Grolimund, D.; Kendelewicz, T.; Trainor, T.P.; Liu, P.; Fitts, J.P.; Chambers, S.A.; Brown, G.E., Jr. *J. Synchrotron Rad*. **1999**, *6*, 612.
76. Dzombak, D.A.; Morel, F.M.M. *Surface Complexation Modeling: Hydrous Ferric Oxide*, Wiley-Interscience, New York, 1990.
77. Charlet, L.; Manceau, A.A. *J. Coll. Interf. Sci.* **1992**, *148*, 443.
78. Chisholm-Brause, C.J.; O'Day, P.A.; Brown, G.E., Jr.; Parks, G.A. *Nature* **1990**, *348*, 528.
79. Towle, S.N.; Bargar, J.R.; Brown, G.E., Jr.; Parks, G.A.; Barbee, T.W., Jr. *Mater. Res. Soc. Symp. Proc*. **1995**, *357*, 23.
80. Towle, S.N.; Bargar, J.R.; Brown, G.E., Jr.; Parks, G.A. *J. Colloid Interface Sci.* **1999**, ***217***, 312-321.
81. Eggleston, C.M.; Stumm, W. *Geochim. Cosmochim. Acta* **1993**, *57*, 4843.
82. Kendelewicz, T.; Liu, P.; Doyle, C.S.; Brown, G.E., Jr. *Surf. Sci.* (sub-mitted).
83. Parks, G.A. *Chem. Rev.* **1965**, *65*, 177; Sverjensky, D.A. *Geochim. Cosmochim. Acta* **1994**, *58*, 3123.

F. McCafferty, E.; Bernett, M.K.; Murday, J.S. *Corrosion Sci.* **1988**, *28*, 559.
G. Amonette, J.E.; Foster-Mills, N.S. (in preparation).

B. Project Productivity

This project accomplished several of the goals stated in the original proposal. Specifically, we conducted detailed experimental studies of the clean surface structure, interaction with water, and redox chemistry of chromate on well-defined iron oxide surfaces. The modeling component of the project did not get to the point of being able to calculate electron transfer rates at the chromate/iron oxide interface, because the less complex calculations involving clean and hydroxylated surface structure proved to be far more difficult that originally envisioned. Likewise, the work on manganese oxide surfaces was just beginning when the project ended. We learned how to grow epitaxial films of β-MnO_2, and studies of the interaction with water with manganese oxide were just beginning when the project ended. The iron oxide research proved to be very time consuming and most of the programmatic resources were spent on this component of the work.

C. Personnel Supported

1. Staff – S.A. Chambers (PNNL), G.E. Brown, Jr. (Stanford), J.E. Amonette (PPNL), N.S. Foster-Mills (PPNL), S.A. Joyce (PPNL), T.J. Kendelewicz (SSRL), J.R. Rustad (PNNL), S. Thevuthasan (PNNL).

2. Postdocs – S.A. Foster Mills (until she converted to staff -- PNNL), S.I. Yi (PNNL), P. Liu (Stanford), D. Grolimund (Stanford).

3. Students – Brian William (PPNL), Collin Doyle (Stanford).

D. Interactions – Conference Papers Presented

1. S. Thevuthasan, G.S. Herman, Y.J. Kim, Y.Gao, S.A. Chambers, N.R. Shivaparan, R.J. Smith, B.J. Morris, and T.T. Tran, "Ion Scattering Studies of Epitaxially Grown Iron Oxide Films on MgO and Al_2O_3 Substrates", 44th National Symposium of the American Vacuum Society, San Jose, CA, October 1997.

2. W. Jiang, S.Thevuthasan, Y.J. Kim, S.A. Chambers, G.S. Herman, D.E. McCready, N.R. Shivaparan, and R.J. Smith, "Mg and Fe Diffusion at the γ-Fe_2O_3(001)/MgO Interface", American Physical Society March Meeting, Los Angeles, CA, March 1998.

3. S. Thevuthasan, Y.J. Kim, S.A. Chambers, P. Liu, T. Kendelewicz, D.E. Brown Jr., J. Morais, R. Denecke, and C.S. Fadley, "Surface Structure Determination of Hematite Using Low-Energy X-Ray Photoelectron Diffraction", S. Thevuthasan, Y.J. Kim, S.A. Chambers, P. Liu, T. Kendelewicz, D.E. Brown Jr., J. Morais, R. Denecke, and C.S. Fadley, American Physical Society March Meeting, Los Angeles, CA , March 1998.

4. *(invited)* J. R. Rustad and D.A. Dixon, "Surface hydrolysis of Fe, Cr, and Al oxides", Physical Chemistry Division, University of Washington, April, 1998.

5. *(invited)* S.A. Chambers, "Surface and Interface Structure of MBE-Grown Fe and Mn Oxides", Naval Research Laboratories, Washington D.C., May 1998 .

6. *(invited)* S.A. Chambers, "Surface and Interface Structure of MBE-Grown Fe and Mn Oxides", Department of Physics, University of Maine, Orono, Maine, May 1998.

7. *(invited)* J.R. Rustad,"The Effectiveness of an Ionic Model Describing Oxyanion Sorption on Ferric Oxide Surfaces", Annual Symposium of the Clay Minerals Society, June, 1998.

8. S. Thevuthasan, Y.J. Kim, S.A. Chambers, P. Liu, T. Kendelewicz, G.E. Brown Jr., J. Morais, R. Denecke, and C.S. Fadley, "The Surface Structure Determination of α-Fe_2O_3 by Intermediate-Energy X-Ray Photoelectron Diffraction", 20th Surface Analysis/10th Annual Pacific Northwest AVS Symposium, Richland, WA, June 1998.

9. W. Jiang, S. Thevuthasan, D.E. McCready, and S.A. Chambers, "Rutherford Backscattering and Channeling Studies of Mg and Fe Diffusion at the Interface of γ-Fe_2O_3(001)/MgO(001), 20th Surface Analysis/10th Annual Pacific Northwest AVS Symposium, Richland, WA, June 1998.

10. D.E. McCready, S. Thevuthasan, W. Jiang, Y.J. Kim, Y. Gao, S.A. Chambers, N.R. Shivaparan, and R.J. Smith , "Rutherford Backscattering and Channeling Studies of Epitaxially Grown Iron Oxide Films on Various Substrates", 20th Surface Analysis/10th Annual Pacific Northwest AVS Symposium, Richland, WA, June 1998.

11. S.A. Joyce and S.A. Chambers, "The Microscopic Structure of Iron Oxide Surfaces", 20th Surface Analysis/10th Annual Pacific Northwest AVS Symposium, Richland, WA, June 1998.

12. S.A. Chambers, "Epitaxial Growth of Ultrathin β-MnO_2 on TiO_2(110) by Oxygen-Plasma-Assisted Molecular Beam Epitaxy", 20th Surface Analysis/10th Annual Pacific Northwest AVS Symposium, Richland, WA, June 1998.

13. N.S. Foster-Mills, J.E. Amonette and S.A. Chambers, "Aqueous Sorption of Cr(VI) on Hematite Using Laser Photoacoustic Spectroscopy", 20th Surface Analysis/10th Annual Pacific Northwest AVS Symposium, Richland, WA, June 1998.

14. *(invited)* S.A. Chambers, S. Thevuthasan, Y.J. Kim, S.A. Joyce, and Y. Liang, "Surface Structure Determination of MBE Grown Iron and Manganese Oxides", National Meeting of The American Chemical Society, Boston MA, August 1998.

15. D. Grolimund, T. Kendelewicz, T.P. Trainor, P. Liu, J.P. Fitts, and G.E. Brown, Jr., "Identification of Cr Species at the Solution-Hematite Interface after

Cr(VI)-Cr(III) Reduction Using GI-XAFS and Cr L-edge NEXAFS", *Xth International XAFS Conference*, Chicago, IL, August 1998.

16. T. Kendelewicz, P. Liu, G.E. Brown, Jr., E.J. Nelson, and S.A. Chambers, "Reaction of Water with Clean (0001) and (1-102) Surfaces α-Fe_2O_3", *14th International Vacuum Congress*, Birmingham, U.K., August 1998.

17. T. Kendelewicz, P. Liu, G.E. Brown, Jr., E.J. Nelson, and S.A. Chambers, "Reduction of the (0001) Surface of Hematite (α-Fe_2O_3) Prepared Under UHV Conditions", *14th International Vacuum Congress*, Birmingham, U.K., August 1998.

18. T. Kendelewicz, P. Liu, G.E. Brown, Jr., E.J. Nelson, and S.A. Chambers, "Fe $L_{2,3}$ and O K Near Edge Structure of Iron Oxides and Hydroxides", *14th International Vacuum Congress*, Birmingham, U.K., August 1998.

19. T. Kendelewicz, P. Liu, G.E. Brown, Jr., and E.J. Nelson, "Reaction of Water with (100) and (111) Surfaces of Magnetite (Fe_3O_4)", *14th International Vacuum Congress*, Birmingham, U.K., August 1998.

20. T. Kendelewicz, P. Liu, G.E. Brown, Jr., E.J. Nelson, M.I. McCarthy, and S.A. Chambers, "Spectroscopic Studies of the Reaction of Water with Metal Oxide Surfaces", Goldschmidt Conference, Toulouse, France, August 1998.

21. S. Thevuthasan, "Rutherford Backscattering and Channeling Studies of Al and Mg Diffusion in Iron Oxide Thin Films", Fifteenth International Conference on the Application of Accelerators, Denton, Texas, November 1998 *(invited*).

22. S. Thevuthasan, Y.J. Kim, S.A. Chambers, P. Liu, T. Kendelewicz, D.E. Brown Jr., J. Morais, R. Denecke, and C.S. Fadley, "The Surface Structure Determination of α-Fe_2O_3 by Intermediate-Energy X-Ray Photoelectron Diffraction", Surface Analysis/8th Annual Pacific Northwest Symposium, June 1998.

23. D.E. McCready, S. Thevuthasan, W. Jiang, Y.J. Kim, Y. Gao, S.A. Chambers, N.R. Shivaparan, and R.J. Smith, "Rutherford Backscattering and Channeling Studies of Epitaxially Grown Iron Oxide Films on Various Substrates", Surface Analysis/8th Annual Pacific Northwest Symposium, June 1998.

24. S. Thevuthasan, W. Jiang, D.E. McCready, and S.A. Chambers, "Rutherford Backscattering and Channeling Studies of Al and Mg Diffusion in Iron Oxide Thin Films", 45th National Symposium of the American Vacuum Society, November 1998.

25. S. Thevuthasan, Y.J. Kim, S.A. Chambers, J. Morais, R. Denecke, C.S. Fadley, P. Liu, T. Kendelewicz, and D.E. Brown Jr., "The Surface Structure Determination of α-Fe_2O_3(0001) by Low-Energy X-Ray Photoelectron Diffraction", 45th National Symposium of the American Vacuum Society, November 1998.

26. S. Thevuthasan, D.E.McCready, W. Jiang, S.I. Yi, and S.A. Chambers, "Ion Beam Analysis of Interface Reactions in Iron Oxide Thin Films", Fourteenth International Conference on Ion Beam Analysis (IBA-14), Dresden, Germany, July 1999 *(invited*).

27. S.A. Chambers, S. Thevuthasan, Y.J. Kim, S.A. Joyce, and Y. Liang, "Surface Structure Determination of MBE Grown Iron and Manganese Oxides", National Meeting of The American Chemical Society, Boston MA, August, 1998 *(invited*).

28. S.A. Chambers, "Molecular Beam Epitaxial Growth and Surface Structure Determination of Fe and Mn Oxides", Center for Catalysis and Surface Structure, Northwestern University, Evanston, Illinois, October 1998 *(invited*).

29. S.A. Chambers and Y. Liang, "Growth of β-MnO_2 Films on TiO_2(110) by Oxygen-Plasma-Assisted Molecular Beam Epitaxy", 45th International Symposium of the American Vacuum Society, Baltimore, Maryland, November 1998.

30. J. R. Rustad, E. Wasserman, and S. A. Joyce, "Structure and Energetics of the Magnetite(001) Surface *Insights From Molecular Dynamics Calculations*", ACS Meeting, Anaheim, CA., March 1999.

31. J. R. Rustad , "Molecular simulation of the iron oxide-water interface", ACS Meeting, New Orleans, LA, August 1999 *(invited*).

32. J.E. Amonette, N.S. Foster, B.K. William, and A.E. Taylor. "Trace-level Chromate Sorption Dynamics at Hematite Surfaces: A Spectroscopic Approach." 217th National Meeting of the American Chemical Society, Anaheim, CA, March, 1999.

33. J.E. Amonette, N.S. Foster, B.K. William, and A.E. Taylor. "Competitive Trace-Level Sorption of Chromate and Phosphate to Hematite Surfaces: A Spectroscopic Approach" 36th Annual Meeting of the Clay Minerals Society, Purdue University, West Lafayette, IN, June, 1999.

34. S.A. Joyce, S. Thevuthasan, and S.A. Chambers, "Growth and Structure of Synthetic Iron Oxide Mineral Surfaces", 217th National Meeting of the American Chemical Society, Anaheim, CA, March 21-25, 1999.

35. T. Kendelewicz, P. Liu, G. E. Brown, Jr., E. J. Nelson, and S. A. Chambers, "Reaction of water with clean (0001) and (1-102) surfaces of α-Fe_2O_3." International Conference on Surface Science 10, Birmingham, UK, August 1998.

36. T. Kendelewicz, P. Liu , G. E. Brown, Jr. , and E. J. Nelson, "Reaction of water with (100) and (111) Surfaces of Magnetite (Fe_3O_4)." International Conference on Surface Science 10, Birmingham, UK, August 1998.

37. T. Kendelewicz, P. Liu , G. E. Brown, Jr., E.J. Nelson, and S. A. Chambers, "Fe $L_{2,3}$ and O K near edge structure of iron oxides and hydroxides." International Conference on Surface Science 10, Birmingham, UK, August 1998.

38. T. Kendelewicz , P. Liu , G. E. Brown, Jr. , E.J. Nelson, and S. A. Chambers, "Reduction of the (0001) surface of hematite (α-Fe_2O_3) prepared under UHV conditions." International Conference on Surface Science 10, Birmingham, UK, August 1998.

39. D. Grolimund, T. Kendelewicz, T. P. Trainor, P. Liu, J. P. Fitts, G. E. Brown, Jr., and S.A. Chambers, "Identification of Cr Species at the solution-hematite interface after Cr(VI)-Cr(III) reduction using GI-XAFS and Cr L-edge NEXAFS." 10th International XAFS Conference, Chicago, IL, July, 1998.

40. T. Kendelewicz, P. Liu, G. E. Brown, Jr., S.A. Chambers, and M.I. McCarthy, "Hydroxylation of the surfaces of simple metal oxides: spectroscopic and thermodynamic analysis." Goldschmidt Conference, Toulouse, France, August, 1998.

41. D. Grolimund, J. P. Fitts, T. P. Trainor, G. E. Brown, Jr., and S.A. Chambers, "Identification of Cr species at the aqueous solution-oxide interface using grazing-incidence XAFS." 217th American Chemical Society Meeting, Anaheim, CA, March, 1999.

42. G.E. Brown, Jr., J. R. Bargar, S.-F. Cheah, C. S. Doyle, D. Grolimund, J. P. Fitts, A. L. Foster, T. Kendelewicz, C. Kim, P. Liu, J. D. Ostergren, G. A. Parks, A. Templeton, H. A. Thompson, S. N. Towle, T. P. Trainor, and S.A. Chambers, "Characterization of adsorbed chemical species at mineral surfaces." 217th American Chemical Society Meeting, Anaheim, CA, March, 1999.

43. S.A. Chambers, S. Thevuthasan, and S.A. Joyce, "Structure and Reactivity of MBE-Grown Fe Oxides", First International Conference on Oxide Surfaces, Elmau, Germany, January 1999 *(invited).*

44. S.A. Chambers, S. Thevuthasan, S.A. Joyce, B. Stanka, and U. Diebold, "Surface Structure of MBE-Grown $Fe_3O_4(001)$ and α-$Fe_2O_3(001)$ by Photoelectron Diffraction and Scanning Tunneling Microscopy", Sixth International Conference on the Structure of Surfaces, Vancouver, British Columbia, Canada, July 1999 *(invited).*

45. S.A. Chambers, G.E. Brown, Jr., T. Kendelewicz, P. Liu, C. Doyle, Y.J. Kim, S. Thevuthasan, S.A. Joyce, J. Morais, R. Denecke, C.S. Fadley, B. Stanka, and U. Diebold, " Structure and Redox Chemistry of Well Defined Iron Oxide Surfaces", Annual Users Meeting of the LBNL Advanced Light Source, Berkeley, California, October 1999 *(invited).*

46. S.A. Chambers, G.E. Brown, Jr., T. Kendelewicz, P. Liu, C.S. Doyle, S. Thevuthasan, S.A. Joyce, B. Stanka and U. Diebold, "Surface Structure and Redox Chemistry of Model Iron Bearing Minerals", Departments of Biology and Chemistry, George Fox University, Newberg, Oregon, February 2000 *(invited).*

47. S.A. Chambers, G.E. Brown, Jr., T. Kendelewicz, P. Liu, C.S. Doyle, S. Thevuthasan, S.A. Joyce, J. Morais, R. Denecke, C.S. Fadley, B. Stanka and U. Diebold, " Surface Structure and Redox Chemistry of Well Defined Iron Oxides", 83rd National Conference of the Canadian Society of Chemistry, Calgary Alberta, Canada, May 2000 *(invited).*

A. Future Work

This project represents the first of what should be several properly funded molecular-level investigations of contaminant/mineral interface chemistry. Much of the work carried out on this program has broken new ground in the rapidly emerging field of molecular environmental science. The number of invited talks at major conferences listed above attests to this fact, as does the fact that this program was one of the few EMSPs started in 1996, and presented at the EMSP Symposium held at the August 1999 National ACS Meeting in New Orleans, to be invited to write a special review paper for the ACS Symposium Proceedings, edited by Gary Eller of LANL. As mentioned in Section VB, we did not have the time or resources to pursue the redox chemistry of contaminants on manganese oxide surfaces, also an important topic in the quest to understand contaminant fate and transport in the subsurface environment. However, a subset of the present investigators (Brown and Chambers, in collaboration with John Zachara of PNNL and Carrick Eggleston of the University of Wyoming) were able to get a new EMSP program funded in 1999 to investigate the role of carbonate layers in mediating the redox chemistry of chromate on iron oxide surfaces. So, the work started he present EMSP program will continue, albeit at a reduce scope.